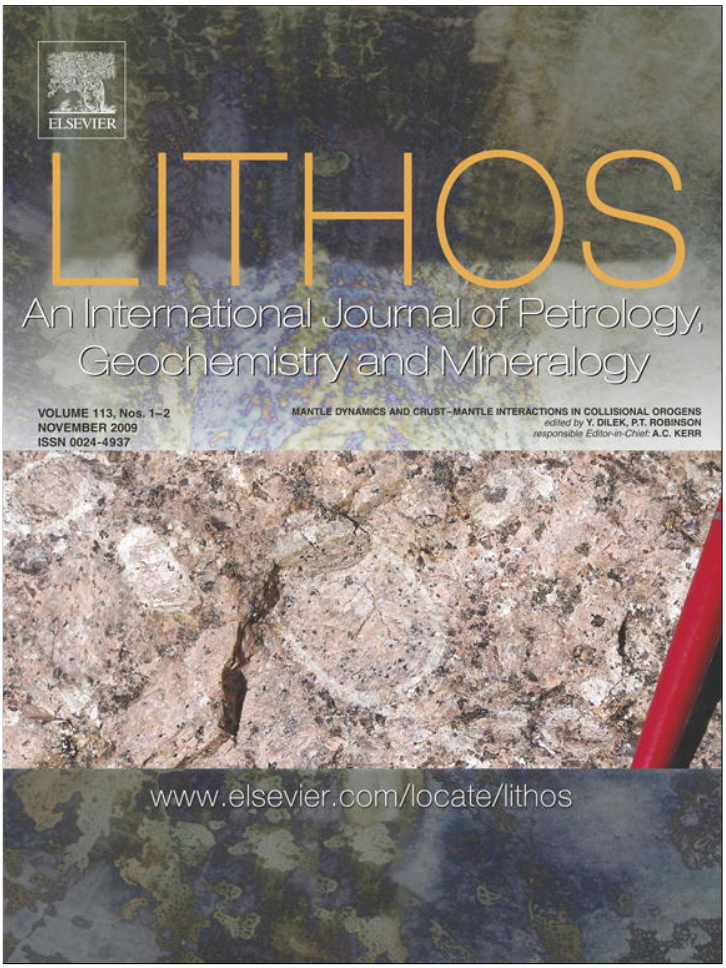

Lithos 113 (2009) 68–87

Contents lists available at ScienceDirect

Lithos

journal homepage: www.elsevier.com/locate/lithos

Island arc tholeiite to boninitic melt evolution of the Cretaceous Kizildag (Turkey) ophiolite: Model for multi-stage early arc–forearc magmatism in Tethyan subduction factories

Yildirim Dilek [a,*], Peter Thy [b]

[a] Department of Geology, 116 Shideler Hall, Miami University, Oxford, OH 45056, USA
[b] Department of Geology, University of California, Davis, CA 95616, USA

ARTICLE INFO

Article history:
Received 5 August 2008
Accepted 27 May 2009
Available online 28 June 2009

Keywords:
Tethyan ophiolites
Kizildag ophiolite (Turkey)
Suprasubduction zone
Protoarc–forearc magmatism
Island arc tholeiite
Boninites

ABSTRACT

The Kizildag ophiolite in Turkey is a remnant of the late Cretaceous suprasubduction zone (SSZ) oceanic lithosphere that was developed in Southern Tethys, and is part of a peri-Arabian ophiolite belt including the Troodos (Cyprus), Baër-Bassit (Syria) and Semail (Oman) ophiolites in the eastern Mediterranean region. The internal structure, petrology and geochemistry of the Kizildag intrusive and extrusive rocks show a magmatic progression from island arc tholeiite (IAT) to boninitic compositions. Similar structural architecture and geochemical trends in the coeval Troodos and Baër-Bassit ophiolites suggest that this multi-stage SSZ magmatism was common in most Tethyan ophiolites. The sheeted dikes and the majority of extrusive rocks in Kizildag are composed of basalt, basaltic andesite and andesite with relatively low La/Sm_N (0.5–0.7), low MgO (7–9 wt.%) and high TiO_2 (0.7–1.0 wt.%) and exhibit high Dy/Yb_N ratios. These IAT suites also include rare, younger dacitic dikes showing strong enrichment in the LREE. The late-stage basaltic dikes and lavas (sakalavites) have high La/Sm_N (0.8–1.0), high MgO (9–11 wt.%) and low-TiO_2 (0.3–0.4 wt.%) contents and display strong depletion in both LREE and HREE. This suite of rocks represents the boninitic component of the Kizildag ophiolite that developed from shallow and greater degrees of melting of hydrous and highly refractory peridotites beneath the extended forearc environment. The progressive evolution of Kizildag magmas from IAT to boninitic compositions in time and space was a result of variable mixing, aggregation, and differentiation of geochemically different melt batches, which formed in different levels (polybaric) within the melting column. Rapid slab rollback-induced corner flow, mantle return flow, and asthenospheric diapirism (providing more fertile melt) directly affected the evolution of this melting column and may have triggered advanced degrees of shallow melting of the hydrous and highly depleted forearc mantle, producing refractory liquids of the boninitic stage. These geochemical patterns of the Kizildag ophiolite reflect a multi-stage evolution of SSZ magmatism in Tethyan subduction factories that is analogous to the earlier arc volcanism in the Eocene–Oligocene Izu–Bonin–Mariana system.

1. Introduction

Recent systematic studies of suprasubduction zone (SSZ) ophiolites have shown that their mafic–ultramafic rock assemblages may be heterogeneous in age and compositions indicating a complex melt evolution of their magmas in nested tectonic settings above a subduction zone; these SSZ ophiolites likely formed in initial stages of subduction zone development during the closure of ocean basins (Beccaluva et al., 1994; Bédard et al., 1998; Shervais, 2001; Godard et al., 2003; Dilek and Flower, 2003; Encarnacion, 2004; Dilek et al., 2005). This scenario is similar to that documented from the in-situ forearc oceanic crust in the intra-oceanic Izu–Bonin–Mariana (IBM) subduction system (Stern and Bloomer, 1992; Bloomer et al., 1995) that displays a typical Penrose-type ophiolite pseudostratigraphy as constrained by deep-drilling results at ODP Site 786 (Arculus et al., 1992; Pearce et al., 1992; Van der Lann et al., 1992; Stern et al., 2003).

The detailed seismic refraction/reflection study of the IBM forearc crust has shown the existence of a thin sedimentary layer (~<200 m) underlain by a 1–2 km-thick layer, composed of fractured volcanic rocks and sheeted dikes (Kamimura et al., 2002). About the upper 660 m of these Eocene lavas and dikes were drilled and recovered at ODP Site 786B. The third layer below (with velocities of 4.3–6.1 km/s) varies in thickness from 2 to 5 km and is possibly made of 'tonalitic' rocks. The underlying fourth layer (5.8 to 6.4 km/s) is inferred to be gabbroic in origin and overlies variably serpentinized peridotites (6.8 km/s) in the mantle wedge (Kamimura et al., 2002). This 'ophiolitic' forearc crust of the Eocene IBM is interpreted to have formed via seafloor spreading during the initiation of subduction and to have constituted the igneous

* Corresponding author. Tel.: +1 513 529 2212; fax: +1 513 529 1542.
E-mail address: dileky@muohio.edu (Y. Dilek).

0024-4937/$ – see front matter © 2009 Elsevier B.V. All rights reserved.
doi:10.1016/j.lithos.2009.05.044

basement of an incipient island arc (Arculus et al., 1992; Stern, 2004). These observations and findings suggest that the oceanic crust formed in the forearc to incipient arc setting within a suprasubduction zone should capture a snapshot picture of an episode of asthenospheric upwelling and melting associated with seafloor spreading immediately following subduction initiation (Stern, 2004, and references therein).

Our recent structural and geochemical studies in the Jurassic Mirdita (Albania) and Pindos (Greece) ophiolites have shown a time-progressive evolution of ophiolitic magmas from MORB to island arc tholeiite (IAT) and boninitic compositions stratigraphically upwards and toward the inferred trench (Dilek et al., 2005, 2007, 2008). This geochemical progression through time and space was a result of various degrees of melting of highly heterogeneous and repeatedly depleted mantle source, which was modified by slab-derived fluids and sediments, similar to the evolution of the IBM forearc crust (Van der Lann et al., 1992; Pearce et al., 1992; Bloomer et al., 1995; Cosca et al., 1998; Stern et al., 2003).

Our current study of representative rock samples from the Cretaceous Kizildag ophiolite (Turkey) (Fig. 1) has revealed similar trends, suggesting that the internal structure, chemostratigraphy, and geochemical features of this ophiolite may provide significant clues for forearc melt generation and magma evolution during subduction initiation, and seafloor spreading tectonics in the early stages of basin closure in the Tethys. A systematic structural, petrological, and geochemical study of the tectonic and magmatic evolution of the Kizildag ophiolite presents new insights about *the Subduction Factory*, specifically about the temporal evolution of forearc crust (temporal constraints on changes in magmatic outputs), better characterization and timing of island arc tholeiite to boninite melt generation in the mantle wedge and beneath the SSZ spreading environment, and changes in the age, nature, and evolution of ophiolitic magmas along-strike of the regional ophiolite belt.

In this paper we present new geochemical data from the sheeted dikes, gabbros and extrusive rocks in the Kizildag ophiolite, compare these data and our interpretations to those available from the nearby and coeval Troodos (Cyprus) and Baër-Bassit (Syria) ophiolites, and document the nature of the time-progressive evolution of ophiolitic magmas from IAT to boninitic compositions. We then present a petrogenetic and geodynamic model highlighting the mode and nature of melt evolution beneath extended protoarc–forearc regions that is applicable to most Tethyan ophiolites in the eastern Mediterranean region.

2. Tethyan ophiolites and Kizildag: regional geology and age relations

Tethyan ophiolites in the eastern Mediterranean region occur in several east–west-trending zones separated by continental blocks, metamorphic core complexes, and sedimentary basins around the northern periphery of the Arabian promontory (Fig. 1). These ophiolites represent remnants of the Tethyan seaways that were obducted in the latest Cretaceous by a series of collisions of intra-oceanic arc-trench systems with continental margins (Dilek et al., 1999; Dilek and Thy, 2006). Following the emplacement of ophiolites, continued subduction of the Tethyan ocean floor in these seaways resulted in the terminal collision and suturing of the bounding

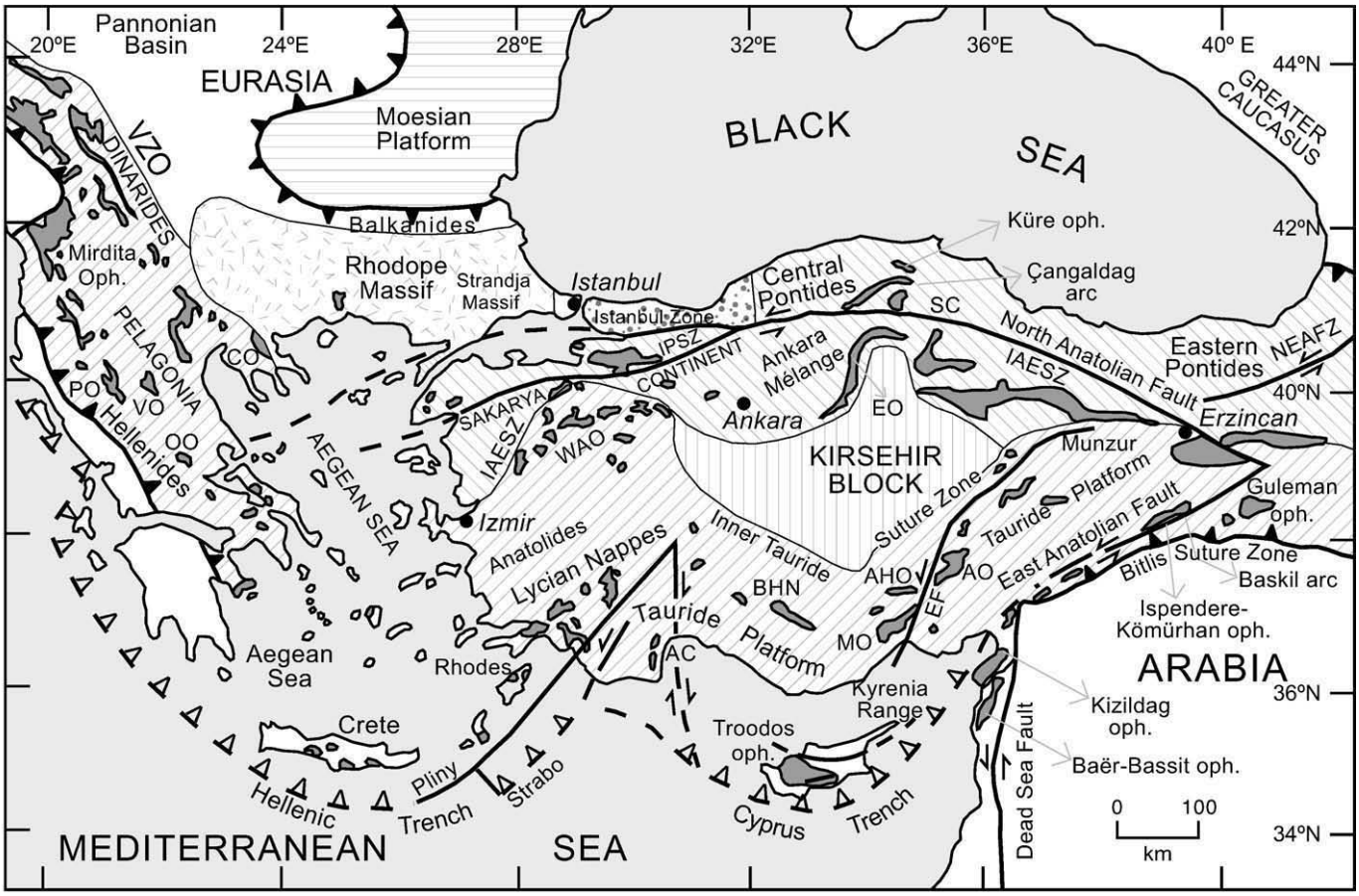

Fig. 1. Tectonic map of the Eastern Mediterranean region showing the distribution of Tethyan ophiolites (shown in dark gray) and major plate boundaries (modified from Dilek and Thy, 2006). Key to lettering: AC—Antalya Complex, AHO—Alihoca ophiolite, AO—Aladag ophiolite, EF—Ecemis fault, EO—Eldivan ophiolite, IAESZ—Izmir–Ankara–Erzincan suture zone, IPSZ—Intra-Pontide suture zone, MO—Mersin ophiolite, NEAFZ—Northeastern Anatolian fault zone, PO—Pindos ophiolite, SC—Sakarya Continent, VO—Vourinos ophiolite, VZO—Vardar Zone ophiolites, WAO—Western Anatolian ophiolites.

Table 1
U–Pb isotopic data for zircons from a plagiogranite dike in the Kizildag ophiolite, Turkey.

Sample	Concentration (ppm)		Isotopic compositions			Calculated ages (Ma)		
97-KD-35	[U]	[Pb]	208/206	207/206	204/206	206*/238	207*/235	207*/206
200–325 m	126.33	1.6911	0.33146	0.05758	0.00066	70.834	71.48	93.01
140–200 m	114.62	1.7623	0.31787	0.05177	0.00026	83.074	83.42	93.41
>140 m	104.65	1.7502	0.30549	0.04954	0.00011	91.557	91.78	97.58

Zircon fractions were separated by standard Wilfley table, heavy liquid, and magnetic mineral separation techniques. Final zircon fractions were sieved and handpicked for purity. The sample labels refer to the sieve screen mesh sizes used to collect the sample fraction. Samples were washed in warm distilled 8 N HNO_3 for 30 min, rinsed in Nanopure H_20 and distilled acetone. Acid-washed zircon fractions were dissolved in a 10 to 1 mixture of doubly distilled HF and 16N HNO_3 in Teflon capsules for 3 to 5 days at 225 °C. The remaining steps in the processing and purification of Pb and U from zircon follow the method of Krogh (1973). The U and Pb isotopic ratios were measured in the static mode on a Micromass Sector 54 thermal ionization mass spectrometer equipped with 7 Faraday cups and an ion-counting Daly detector, using single Re filaments and standard P_2O_5-silica gel loading techniques for Pb and U. Corrections of measured isotopic ratios for blank and fractionation, and the calculation of Pb and U concentrations were performed using the PBDAT software (Ludwig, 1990). Errors reported are % 2s. Initial common Pb compositions were estimated using the two-stage Pb evolution model of Stacy and Kramers (1975). Regressions were calculated and plotted using ISOPLOT (Ludwig, 2003), with corrected Pb/U ratios, rho values, and calculated errors obtained from PBDAT (Ludwig, 1990). Uncertainties in age are reported at the 95% confidence level. Concentrations were determined with a mixed ^{208}Pb–^{235}U spike. The Pb isotopic compositions was corrected for mass fractionation and bias using a factor of 0.10 ± 0.05% per AMU based on replicate analyses of NIST SRM 981 and SRM 983. All decay constants conform to the values recommended by Steiger and Jager (1977). The data was also corrected for U (0.01 ng) and Pb (0.20 ng) procedural blanks with Pb 206, 207, 208:204 = 19.4, 15.9, 39.3. *Pb denotes radiogenic Pb.

continental blocks by the middle-late Eocene (Dewey et al., 1986; Dilek and Moores, 1990).

The Cretaceous ophiolites occurring south of the Tauride platform in southern Turkey (Fig. 1) were derived from the Southern Tethys, and were emplaced southward onto the northern edge of the Arabian continent. These include the peri-Arabian ophiolites (*le croissant ophiolitique péri-arabe*) of Ricou (1971) along the Bitlis–Zagros suture zone in Turkey and Iran, namely the Kizildag (Turkey), Baër-Bassit (Syria), Kermanshah and Neyriz (Iran). The Troodos ophiolite to the west has been in the process of emplacement since the latest Miocene–Pliocene (Robertson, 1998) onto the Eratosthenes seamount, which has been partially subducted along the Cyprus trench.

All these ophiolites, including the Semail in Oman, are nearly coeval in age and are likely to have developed within a laterally continuous (in an ~ESE direction in the present coordinate system) arc-trench rollback system in the Southern Tethys (Robertson, 2002; Dilek and Flower, 2003). The Troodos, Baër-Bassit, and Kizildag ophiolites are particularly important for displaying field evidence for original seafloor spreading tectonics and magmatic processes associated with oceanic crust formation in an extended arc–forearc setting, because they have escaped the intense Miocene and younger deformation due to the Arabian continental collision. The U–Pb zircon dating of two plagiogranite intrusions in the Troodos plutonic complex has revealed crystallization ages between 90.3 ± 0.7 Ma and 92.4 ± 0.7 Ma (Mukasa and Ludden, 1987). These igneous ages are consistent with the radiolarian stratigraphy ages of 89–91 Ma from the umberiferous strata overlying the Troodos extrusive sequence (Blome and Irwin, 1985). New precise ^{40}Ar–^{39}Ar hornblende dating of amphibolite samples from the Mamonia Complex in SW Cyprus has yielded plateau ages of 75.7 ± 0.3 Ma to 88.0 ± 0.8 Ma (Chan et al., 2007) that are interpreted as the timing of subduction–accretion metamorphism beneath the Troodos oceanic crust. The maximum, subduction-related metamorphic age (~88 Ma) is nearly contemporaneous with the igneous development of the ophiolite.

Systematic and reliable age data from the Baër-Bassit ophiolite are lacking. K–Ar whole rock ages from the sheeted dikes range between 73 Ma and 99 Ma (Delaloye and Wagner, 1984). New ^{40}Ar–^{39}Ar hornblende plateau ages from amphibolites in the metamorphic sole beneath the ophiolite range between 71.7 ± 0.5 Ma and 88.4 ± 0.4 Ma (Chan et al., 2007). The maximum metamorphic age of 88.4 ± 0.4 Ma from the sole is most likely coeval or slightly younger than the igneous development of the Baër-Bassit ophiolite.

Extensive hydrothermal alteration and metamorphism of the crustal units in the Kizildag ophiolite, which is situated ~250 km NE of Troodos–Cyprus, renders the previously reported K–Ar whole rock ages from the pillow lavas (77–44 Ma), dikes and gabbros (116–71 Ma) unreliable (Çogulu et al., 1975; Delaloye et al., 1977). Timing of the tectonic emplacement of the Kizildag ophiolite onto the northern edge of Arabia is constrained as post-Turonian (~90 Ma) and pre-Maastrichtian (~71 Ma) based on the biostratigraphic ages of the sedimentary cover and the underlying shelf strata (see Section 3 below). We have obtained new U–Pb zircon ages from a plagiogranite intrusion crosscutting the sheeted dikes within the Karaçay Valley. Magnetically separated zircon fractions from Sample 97KD-35 have yielded internally and externally concordant U–Pb crystallization ages of 91.8–91.6 Ma (Table 1). These ages are nearly the same as the plagiogranite crystallization ages from Troodos, indicating that the Kizildag, Troodos, and Baër-Bassit ophiolites are contemporaneous and most probably tectonically related within the same SSZ setting.

2.1. Baër-Bassit ophiolite, Syria

The Baër-Bassit ophiolite (BBO), less than 50 km south of Kizildag (Fig. 1), forms a tectonic outlier of a late Cretaceous ophiolite nappe emplaced southward onto the Arabian platform carbonates (Parrot, 1980; Delaloye and Wagner, 1984), and it is highly dismembered and internally disrupted because of its deformation during and after emplacement (Morris et al., 2002). Despite its significant deformation, the Baër-Bassit ophiolite includes all major subunits of an ideal Penrose-type oceanic lithosphere (Fig. 2), and unlike the Kizildag ophiolite it is underlain by imbricate thrust sheets of a metamorphic sole consisting of amphibolite and greenschist rocks (Parrot, 1980; Thuziat et al., 1981; Al-Riyami et al., 2002).

The upper mantle peridotites in the Baër-Bassit ophiolite consist of harzburgite and dunite that are extensively serpentinized. Dunite and chromite pods and lenses become more common higher up in the mantle sequence, where pyroxenite, wehrlite and websterite dikes crosscut the harzburgite and its high-temperature fabric elements (Fig. 2; Al-Riyami et al., 2002). Ultramafic cumulates overlying the tectonized harzburgites are locally preserved in the ophiolite.

The plutonic section includes layered and isotropic gabbros and gabbro pegmatites (Parrot, 1980; Al-Riyami et al., 2002) that occur in limited outcrops. Isotropic gabbro and pegmatitic gabbro are locally intrusive into the tectonized harzburgites. Olivine gabbro is also seen as xenoliths in the isotropic gabbro. There are no detailed geochemical data available from the mantle peridotites and plutonic rocks in the Baër-Bassit ophiolite.

Sheeted dikes crop out in isolated locations, commonly in thrust contact with the other ophiolitic subunits. Where well exposed in a transitional contact with the underlying isotropic gabbros and plagiogranites, sheeted dikes occur as steeply dipping intrusions ranging in thickness from 30 cm to 150 cm and with one- and two-sided chilled margins. They are crosscut by moderately dipping faults (Fig. 2) and are extensively altered. Al-Riyami et al. (2002) do not report different dike generations based on crosscutting relations and variations in chemical compositions, but state based on a limited

geochemical dataset that the majority of the analyzed dike samples are composed of low-TiO_2 magnesian basalts or basaltic andesites with island arc tholeiite (IAT) affinities.

Extrusive rocks in the Baër-Bassit ophiolite occur in thrust sheets in contact mainly with the serpentinized peridotites. A ~400-m-thick lava sequence near the village of Deflah overlies the sheeted dikes and is intruded in its basal section by dike swarms (Al-Riyami et al., 2002). The main rock types include pillow lavas, hyaloclastite breccias, and massive lava flows (rare) that are locally interlayered with and overlain by manganiferous umber deposits (Fig. 2). There is no clear igneous stratigraphy identified within the Baër-Bassit extrusive sequence, as in the Troodos lavas, but Al-Riyami et al. (2002) suggest that the pillow lavas with dike intrusions (Deflah unit) constitute the lower part of the Baër-Bassit extrusives, whereas the lava breccias and hyaloclastites (Baluta unit) make up the upper part. Compositionally, most pillow lavas are basaltic andesites with similar geochemical features as in the sheeted dikes, and the samples reported by Al-Riyami et al. (2002) appear to range from MORB to IAT to boninitic affinities.

2.2. Troodos ophiolite, Cyprus

The Troodos ophiolite north of the Arakapas fault zone consists of a central core of variably serpentinized peridotites overlain by layered to isotropic gabbros, sheeted dikes, and extrusive rocks (Fig. 2). The Troodos extrusive sequence is conformably overlain by the upper Cretaceous chalk deposits, which are unconformably covered by a Maastrichtian–lower Eocene pelagic limestone and the upper Eocene–Oligocene carbonates (Fig. 2). A lower Miocene reefal limestone and the Messinian gypsum-evaporite deposits constitute the youngest marine sedimentary cover above Troodos.

The mantle section in Troodos includes mainly harzburgites with associated lherzolites and dunites (with chromite pods) that are variably serpentinized (Gass, 1990). The harzburgite displays a pervasive foliation defined by the planar alignment of orthopyroxene (opx) and spinel grains, and foliation-parallel segregation of olivine- and orthopyroxene-rich bands. Batanova and Sobolev (2000) subdivided the mantle section into two geochemical units based on the Cr/(Cr + Al) ratio (Cr#) of spinel and the modal abundance of clinopyroxene (cpx). Spinel lherzolite with a Cr# of 0.22–0.28 and 5–7 modal % of cpx occurs in the east-central part of the peridotite body in Troodos and contains numerous dunite pods and cpx-bearing harzburgite. The second unit is composed of cpx-poor refractory harzburgite with a Cr# of 0.51–0.70 and 0.5–1.0 modal % of cpx. This peridotite occurs higher in the mantle sequence and just beneath the ~1-km-thick mafic–ultramafic cumulate section making up the petrological Moho (Fig. 2). The spinel lherzolite formed as residuum after extraction of MORB melts, and was modified by late-stage melts with calc-alkaline and/or boninitic compositions percolating through them, as evidenced by veins and pods of dunite–chromitite and

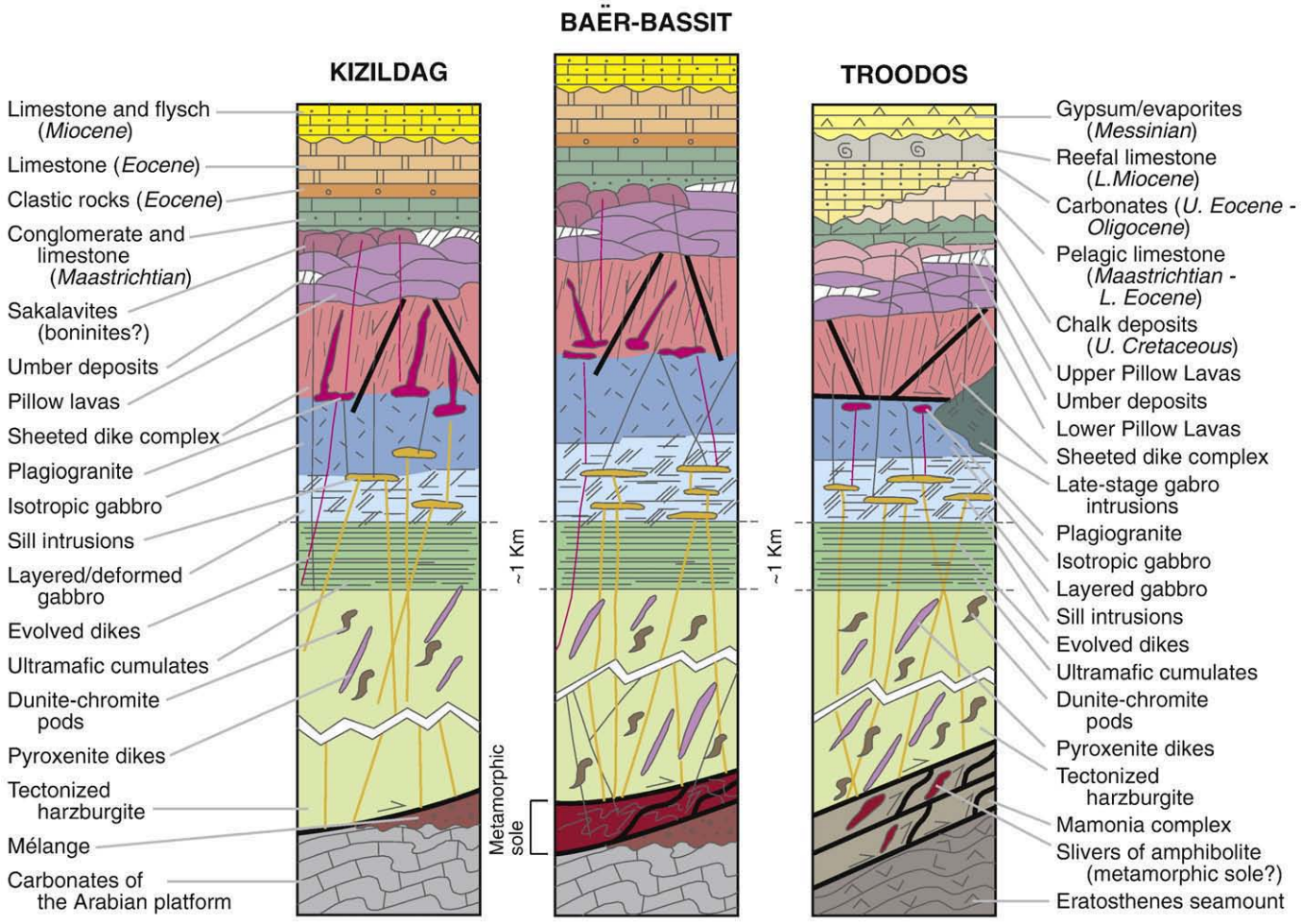

Fig. 2. Composite stratigraphic columnar sections of the Kizildag (Turkey), Baër-Bassit (Syria) and Troodos (Cyprus) ophiolites, showing the igneous layering and stratigraphy, crosscutting relations of different dike generations and contact relations within the ophiolites, and the sedimentary and tectonic units overlying and underlying these ophiolites. Data are from Dilek and Thy (1998) and Erendil (1984) and Tekeli and Erendil (1986) for Kizildag; Al-Riyami et al. (2002) for Baër-Bassit; and, Dilek et al. (1990), Robinson and Malpas (1990), and Thy and Esbensen (1993) for Troodos.

harzburgite (Batanova and Sobolev, 2000). The dominantly harzburgitic peridotites constitute the residuum after the formation of the highly refractory magmas of this late magmatic event.

The plutonic complex consists of two suites of gabbroic rocks, as shown by field mapping and petrological studies of drill cores (Malpas et al., 1989; Thy et al., 1989). The lower suite, which is composed of undeformed plutons, is compositionally and mineralogically similar to the underlying mafic–ultramafic cumulates and is intrusive into the undeformed upper suite (Fig. 2), which is compositionally similar to the sheeted dike complex (Robinson and Malpas, 1990). These intrusive relations combined with the petrological and geochemical observations suggest a two-stage evolution of the Troodos ophiolite. The earlier seafloor spreading produced ophiolite sequence includes the upper plutonic suite, sheeted dikes, and the Lower Pillow Lava (LPL) series (Thy and Esbensen, 1993). This young oceanic lithosphere was subsequently underplated by magma chamber(s) of basaltic andesite compositions that produced the mafic–ultramafic cumulates and depleted Upper Pillow Lava (UPL) series (Fig. 2). Dikes that feed into these UPL have steep dips, and they crosscut the earlier-formed sheeted dikes (Fig. 2; Dilek et al., 1990).

The extrusive sequence in the Troodos ophiolite contains three major geochemical suites (Robinson et al., 1983; Malpas and Langdon, 1984; Robinson and Malpas, 1990; Thy and Xenophontos, 1991; Bednarz and Schmincke, 1994; Portnyagin et al., 1997). A lower suite of relatively evolved island arc tholeiite (IAT) lavas, a middle suite of depleted arc tholeiite rocks, and a stratigraphically higher suite of highly depleted boninitic rocks. The lower suite and the middle and higher suites correspond approximately to the LPL and UPL divisions of the Troodos extrusive sequence (Gass, 1990, and references therein), respectively. Olivine- and olivine + plagioclase-phyric, relatively high-Ti lavas (with MORB-like abundances of primitive to evolved magmas) of the LPL series in the Akaki Canyon area in north-central Troodos are transitional upwards to aphyric and olivine-phyric, low-Ti depleted tholeiitic lavas of the UPL series (Malpas and Langdon, 1984; Dilek and Flower, 2003). The extrusive sequence in the Margi–Kataliondas section farther east in the ophiolite displays a relatively sharp transition from the primitive to evolved LPL series to ultra low-Ti and ultra-depleted, high-Ca boninitic lavas (Dilek and Flower, 2003). These ultra-depleted high-Ca boninitic lavas also occur in the Limassol Forest area to the south, adjacent to the Arakapas fossil transform fault zone (Flower and Levine, 1987).

The sheeted dikes display similar compositional ranges as the different suites in the extrusive sequence without the sharp compositional breaks of the lavas, and the rock types span from basalts to rhyodacites (Baragar et al., 1989). The majority of the sheeted dikes are made of basalt and basaltic andesite, which geochemically correlate with the LPL series (Dilek et al., 1990; Thy and Esbensen, 1993). Thus, sheeted dikes and the LPL series can be considered as the products of an early-stage, spreading related magmatism in the history of the Troodos ophiolite. Both sheeted dikes and lavas are cut by numerous normal faults, some of which contain hydrothermal veins of epidote, quartz, and pyrite. The sheeted dike complex includes several ~N–S-trending structural grabens formed by blocks of inward-dipping dikes and extensional faults, and locally (i.e. in the Solea graben) highly rotated sheeted dikes are separated from the underlying gabbros by low-angle detachment faults (Fig. 2).

3. Geology of the Kizildag ophiolite

3.1. Igneous architecture of Kizildag

The NE–SW trending Kizildag ophiolite consists of a core of serpentinized mantle rocks overlain by a plutonic sequence, sheeted dikes, and extrusive rocks (Fig. 3; Dubertret 1955; Vuagnat and Çogulu, 1967; Çogulu et al., 1975; Selçuk, 1981; Erendil, 1984; Tekeli and Erendil, 1986). It is stratigraphically overlain by a generally east-dipping upper Maastrichtian-Tertiary sedimentary sequence (Figs. 2 and 3). The ophiolite includes two structurally distinct massifs that are separated by the NW-striking Tahtaköprü fault (Fig. 3). The main massif south of this fault contains a NE-trending antiformal peridotite core bounded by crustal units both on the NW and the SE. The 3-km-thick mantle units consist mainly of serpentinized harzburgite tectonite with local bands and lenses of dunite, wehrlite, lherzolite, and feldspathic peridotites (Fig. 2). Relatively undeformed gabbroic to doleritic dikes crosscut the serpentinized mantle rocks (Dilek et al., 1991).

The contact between the mantle rocks and the plutonic sequence is locally sheared and dips away from the ultramafic rocks and beneath the gabbros. Gabbroic rocks above this contact display cumulate textures commonly cut by low-angle mylonitic shear zones and boudinage structures (Fig. 4F, G). These shear zones are millimetric to decimetric in scale and have diffuse to sharp boundaries with the surrounding undeformed gabbros. Isotropic gabbros become predominant upward in the plutonic sequence, as the layered and foliated fabrics in the gabbros disappear. Multiple and mutually intrusive relations between isotropic gabbros and small bodies of plagiogranite, leucocratic gabbro, and dolerite are common in the uppermost part of the plutonic sequence (Dilek and Eddy, 1992). Late-stage, lighter-colored and medium- to coarse-grained intrusions in the layered and isotropic gabbros display jigsaw puzzle-like rip-apart structures suggesting forceful injection of their magmas into the solid host rock (Fig. 4E). Doleritic dike intrusions locally increase towards the top of the 2.5 km-thick plutonic sequence where dikes become predominant and have irregular and commonly diffuse boundaries with the host gabbro (Fig. 4B). Farther up from this zone (within 100 to 150 m) gabbros diminish, and dikes become planar with sharp boundaries with one- and two-sided chilled margins (Fig. 4A, B, C). This local zone of the dike–gabbro transition appears to be the root zone of the sheeted dike complex.

The main outcrop of the sheeted dike complex occurs in a NE–SW-oriented structural graben bounded on both sides by the plutonic sequence (Fig. 3). The dike–gabbro boundary in this graben is locally marked by moderately- to gently-dipping normal faults (Fig. 4D), which are associated with anastomosing brittle–ductile shear zones (Dilek and Eddy, 1992; Dilek and Thy, 1998). This sheared contact between the dike complex and the plutonic sequence is a brittle–plastic transition zone analogous to the detachment surface in the Solea graben of the Troodos ophiolite (Dilek and Eddy, 1992; Hurst et al., 1994). Mineralized oceanic faults transect the dikes and form two major subsets: one subset of faults is parallel to the generally steeply dipping dikes with shallower dip angles and displays down-dip plunging slickenside lineations. Locally, these faults form well-developed horst-graben structures (Fig. 2), whereas in some places they are listric in geometry, associated with rotated and tilted fault blocks of sheeted dike swarms (Dilek and Eddy, 1992).

Crosscutting relations and textural and compositional differences indicate the existence of at least three main generations of dike intrusions in the Kizildag sheeted dike complex. The first generation and the oldest dikes are made of basalt–dolerite and constitute the majority of the steeply to moderately dipping, wall-to-wall sheeted dikes that are crosscut by the oceanic faults described above. These sheeted dikes are intruded by individual dikes and dike swarms of the second generation that are commonly subparallel and/or oblique to their host dikes. They may range in thickness from 20–30 cm to 50–70 cm and are medium- to fine-grained. These intrusions also crosscut the layered and isotropic gabbros and are locally injected into them as medium- to coarse-grained, subhorizontal sills and small stocks (Fig. 4E, F). They are made of basaltic andesite, andesite and rare dacite. The third generation, late-stage dikes crosscut the older dikes at random angles (steeply dipping to subhorizontal) as thin (5 to 25 cm), individual dikes that locally show zig-zag patterns controlled by the distribution of faults, fractures and pre-existing dike margins. These dikes also intrude the isotropic and layered gabbros at various angles (Figs. 2 and 4), and they are made of high-Mg andesites or

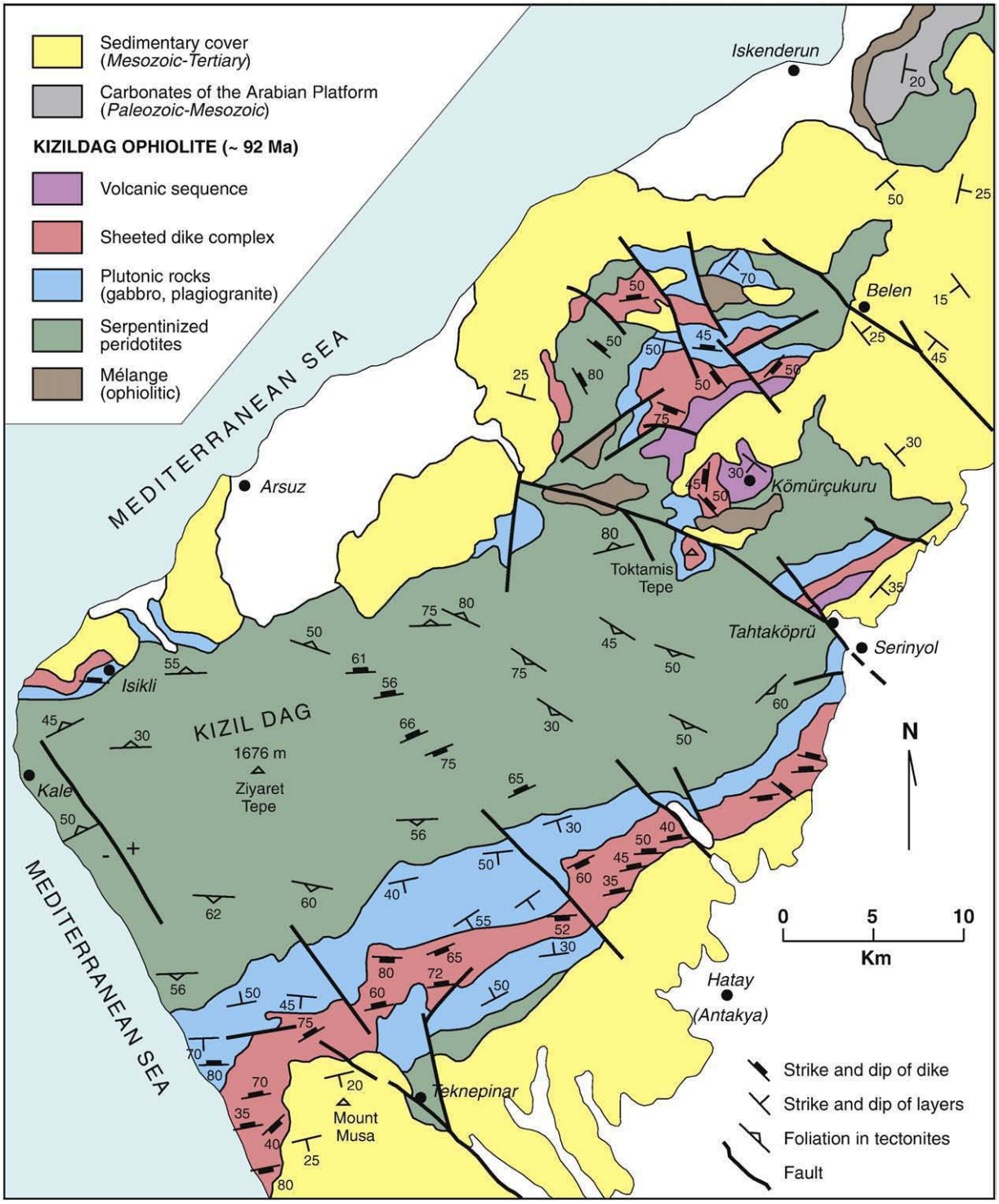

Fig. 3. Simplified geological map of the Kizildag ophiolite (modified from Dilek and Thy, 1998, with additional structural data based on this study).

boninites (see geochemistry below). Plagiogranite dikes show mutual crosscutting relations with both dolerite and basaltic andesite dikes in the sheeted dike complex.

The second massif of the ophiolite, occurring east of the Tahtaköprü fault, lacks the coherent internal structure and stratigraphy observed in the main massif in the southwest. It consists mainly of volcanic, dike, and plutonic rocks directly overlying the serpentinized peridotites (Fig. 3; Dilek and Delaloye, 1992; Dilek and Eddy, 1992). The extrusive sequence crops out in two locations in this massif. One of them near the village of Tahtaköprü includes a ~400-m-thick sequence, consisting of massive and pillow lavas intercalated with hyaloclastites and metalliferous sedimentary rocks. These volcanic rocks overlie serpentinized peridotites along a gently southeast-dipping fault and are in turn overlain stratigraphically by the Maastrichtian siliciclastic and carbonate rocks (Fig. 3). The second exposure of extrusive rocks occurs farther north around the Kömürçukuru village and directly overlies the isotropic gabbros (Fig. 3). This ~600-m-thick block includes mainly pillow and massive lava flows interstratified with metalliferous umbers (Fig. 2; Tekeli and Erendil, 1986; Dilek and Thy, 1998). The umber horizons are locally spatially associated with bleached hydrothermal alteration zones and/or mineralized zones enriched in pyrite, chalcopyrite and malachite (Robertson, 1986).

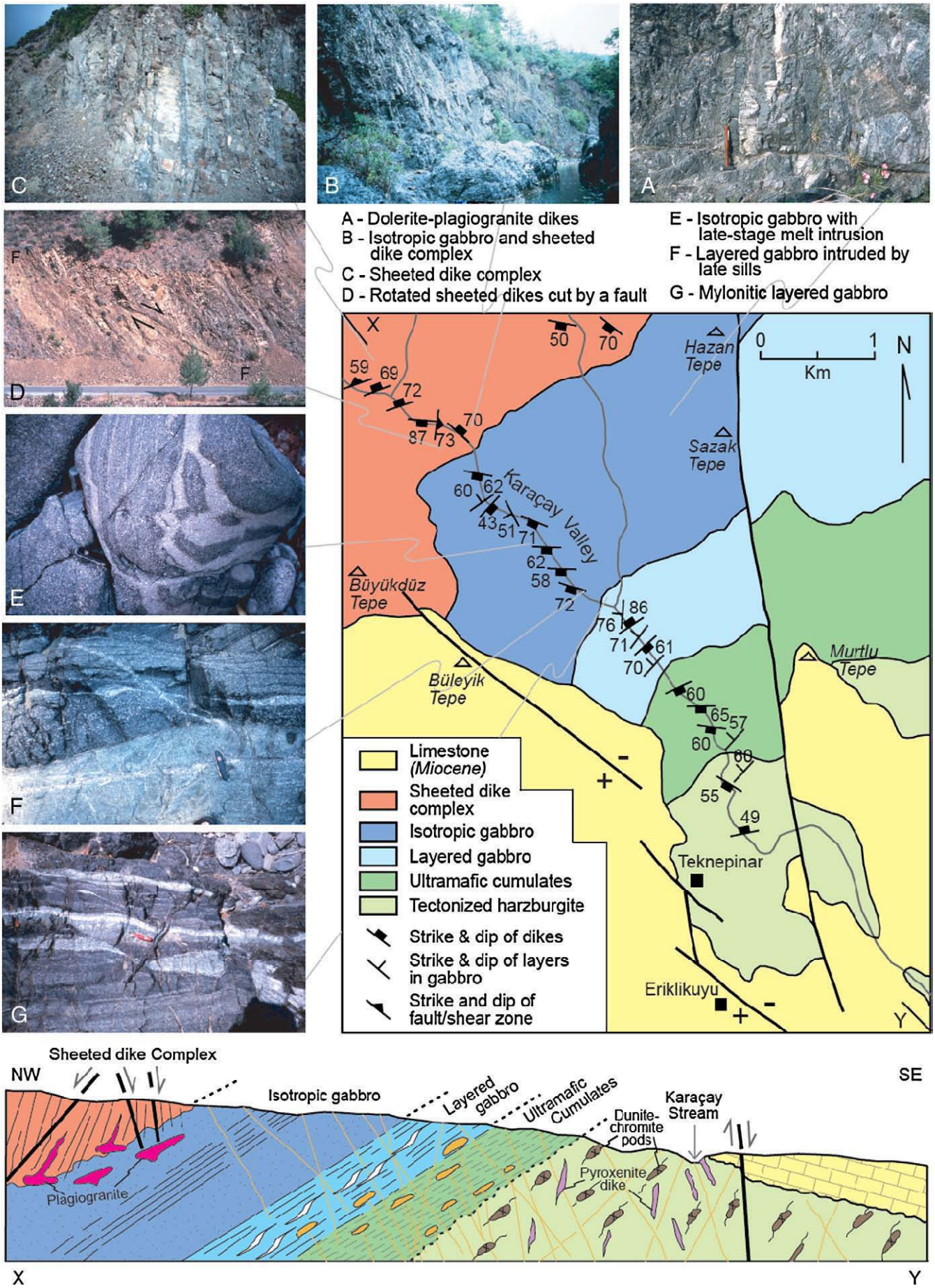

A separate exposure of pillow lavas occurs on the Antakya-Altinözü Road near Mount Silpius, 12 km SE of the main massif of Kizildag, forming a ~300-m-thick volcanic unit. First described by Dubertret (1955) as *sakalavites*, these pillow lavas rest on serpentinized peridotites and are conformably overlain by Campanian claystone, argillaceous sandstone–limestone, and mudstone that are in turn unconformably covered by upper Maastrichtian clastic rocks. Egg-shaped pillow lavas (sakalavites) up to 20 cm in size are embedded in an interstitial hyaloclastite matrix, which also contains micro pillows (4–5 cm long) and nodules (Dubertret, 1955; Laurent et al., 1980). Compositionally, these sakalavites are high-Mg andesites or boninites (see geochemistry below). Their stratigraphic position in the Kizildag ophiolite sequence is not well constrained; however, the existence of the intercalated non-silicified umber deposits that are similar to the ones observed higher up in the Kömürçukuru section (Robertson, 1986) and the overlying Campanian sedimentary rocks suggest that these high-Mg sakalavites may represent the youngest eruptive rocks in the Kizildag ophiolite.

3.2. Seafloor spreading structures in Kizildag and their significance

The Kizildag ophiolite displays well-preserved seafloor spreading structures (Dilek and Delaloye, 1992; Dilek and Eddy, 1992). These include an extensive sheeted dike complex with multiple generations of crosscutting dikes; high- to low-angle mineralized faults (i.e. epidote, chlorite, quartz, hematite) intersecting dikes and pillow lavas; detachment surfaces crosscut by dikes and hydrothermal veins; hydrothermal alteration zones and epidosites in the volcanic sequence and sheeted dike complex reminiscent of hydrothermal discharge zones and black smokers in modern spreading environments; plutonic sequence with 2.5 km of cumulate and layered to isotropic gabbros that display igneous flow and deformation fabrics crosscut by dikes.

The faults in the Kizildag ophiolite are of seafloor spreading origin, rather than tectonic emplacement and/or neotectonic structures as in the Baër-Bassit ophiolite (Morris et al., 2002) because: (1) they are generally mineralized (epidote + chlorite + hematite + albite ± quartz) and show slickenside lineations with down-dip plunge (dike-parallel normal faults); (2) they are crosscut by dikes, dike swarms (mostly andesitic), and hydrothermal veins; (3) faults/shear zones and associated deformed rocks between the peridotites and gabbros and the gabbros and sheeted dikes show shear sense indicators (i.e., S-C fabric, asymmetric porphyroclasts, mini-faults, necking and boudinage) compatible with their extensional origin and are locally cut by pegmatitic gabbro, basaltic dikes, and/or hydrothermal veins; (4) high-angle faults locally form horst-graben structures within the sheeted dike complex; and (5) dike-parallel normal faults in the sheeted dike complex die out in the uppermost part of the underlying gabbros. Points 1 through 3 above indicate that the observed faults and shear zones are of extensional origin formed while magmatism and associated hydrothermal circulation were still active. Points 4 and 5 suggest that faults in the dike complex represent brittle structures that do not extend down into a plastic regime in the mush zone (gabbros below the low velocity zone) beneath the spreading axis.

The seafloor spreading structures in the Kizildag ophiolite resemble those documented both in the Troodos ophiolite (Dilek and Eddy, 1992), in modern oceanic lithosphere at mid-ocean ridges (Dilek et al., 1991; Dilek and Delaloye, 1992; Dilek et al., 1998; Karson, 1998), and in extended modern protoarc–forearc environments (Stern et al., 1989; Taylor et al., 1991; Klaus et al., 1992; Taylor, 1992; Bloomer et al., 1995; Gribble et al., 1996; Cosca et al., 1998; Ishizuka et al., 2002, 2003; Hawkins, 2003; Straub, 2003; Nishizawa et al., 2006; Takahashi et al., 2007). The older oceanic crust in the Izu–Bonin–Mariana (IBM) and Tonga forearc regions, for example, has been stretched and thinned by upper plate extension and has been overbuilt by new arc crust (Klaus et al., 1992; Stern and Bloomer, 1992; Taylor et al., 1991; Bloomer et al., 1995; Cosca et al., 1998). Crustal extension in these settings has been accommodated by high- to low-angle normal faults forming half- and full-grabens. High-angle, graben-bounding faults against the proto-remnant arc become subhorizontal at ~2.8 km depth, suggesting that extensional structures in the forearc–protoarc region are detached at shallow crustal levels (Klaus et al., 1992).

3.3. Units above and below the Kizildag ophiolite

3.3.1. Sedimentary cover

The oldest sedimentary rocks directly overlying the extrusive sequence of the Kizildag ophiolite along an unconformity are the upper Maastrichtian clastic rocks, including basal conglomerate and sandstone that are transitional upward into limestone (Figs. 2 and 5; Selçuk, 1981). This post-emplacement transgressive sequence contains ophiolite-derived detrital material and hippurite and globotruncana species. These upper Maastrichtian rocks are conformably overlain by a nearly 600-m-thick, Paleocene–upper Eocene series composed of sandstone, mudstone, cherty limestone, and recrystallized micritic limestone (Selçuk, 1981). These rocks include fossils of benthic organisms and suggest deeper marine conditions in the Paleocene–Eocene. The Paleogene units are unconformably overlain by a ~1600-m-thick middle to upper Miocene transgressive series consisting of conglomerate, sandstone, mudstone as in a flysch sequence, and reefal limestone and recrystallized limestone (Selçuk, 1981). Both the flysch unit and the limestone units of the Miocene strata locally directly rest on various subunits of the Kizildag ophiolite (i.e., in Teknepinar, Mount Musa, Kömürçukuru, and Belen; Fig. 3). Fossil species of enchinoidea, bryozoa, ostracada, bivalva, and benthic foraminifera are abundant in the Miocene cover rocks and indicate generally shallow marine conditions in the region during this time.

3.3.2. Tectonic units beneath the ophiolite

Highly sheared and serpentinized harzburgites rest tectonically on the Albian–Aptian limestones of the Arabian carbonate platform on a low-angle thrust fault near the village of Kömürçukuru (Figs. 2, 3 and 5). Sandwiched between these two is a mélange, which consists of, from top to bottom, sheared serpentinites containing imbricate thrust sheets of the Cretaceous platform limestones, a sedimentary succession of mudstone, siltstone, sandstone, volcaniclastic rocks, debris flow, and limestone, all of which include ophiolite-derived clastic material, and a bituminous shelf limestone. The limestone unit at the very bottom is laminated and contains interlayers of serpentine mud. This mainly ophiolitic mélange unit beneath Kizildag is likely to have formed in a restricted basin on top of the Arabian platform and in front of the

Fig. 4. Detailed geological map of the Karaçay Valley in the Kizildag ophiolite (center) and field photographs showing various structures in the sheeted dike complex and the plutonic rocks. Geological cross-section below depicts the internal structure and stratigraphy of the ophiolite. A. Intrusive relations of dolerite and plagiogranite dikes within the sheeted dike complex; B. Dike–gabbro transition zone along the Karaçay Valley. The light-colored rock in the foreground is a fine-grained isotropic gabbro, which contains doleritic dikes and dikelets of irregular size and shape. Steeply SE-dipping sheeted dikes in the background are emanating from this transition zone and the underlying plutonic rocks. The dike–gabbro transition zone here is the root zone of the sheeted dike complex. Irregular plagiogranite intrusions seen in A are common both in the isotropic gabbro and the sheeted dikes across this igneous contact. C. Wall-to-wall sheeted dike intrusions composed mainly of the first generation dolerite dikes. D. Moderately- to gently-dipping and altered sheeted dikes, which are cut by and rotated along a gently-dipping normal fault. E. Faintly layered to isotropic gabbros deformed by late-stage andesitic melt intrusions. These intrusions forcefully infiltrated the gabbros, forming rafts of gabbro xenoliths and jigsaw puzzle diking–rifting patterns. F. Ductily deformed, layered gabbros intruded by late-stage andesitic–boninitic dikes, sills and thin stocks. These intrusions are depicted in orange–yellow in the structural cross-section. G. Layered gabbro with mylonitic shear zones that show intense strain localization and boudinaged and necked compositional bands.

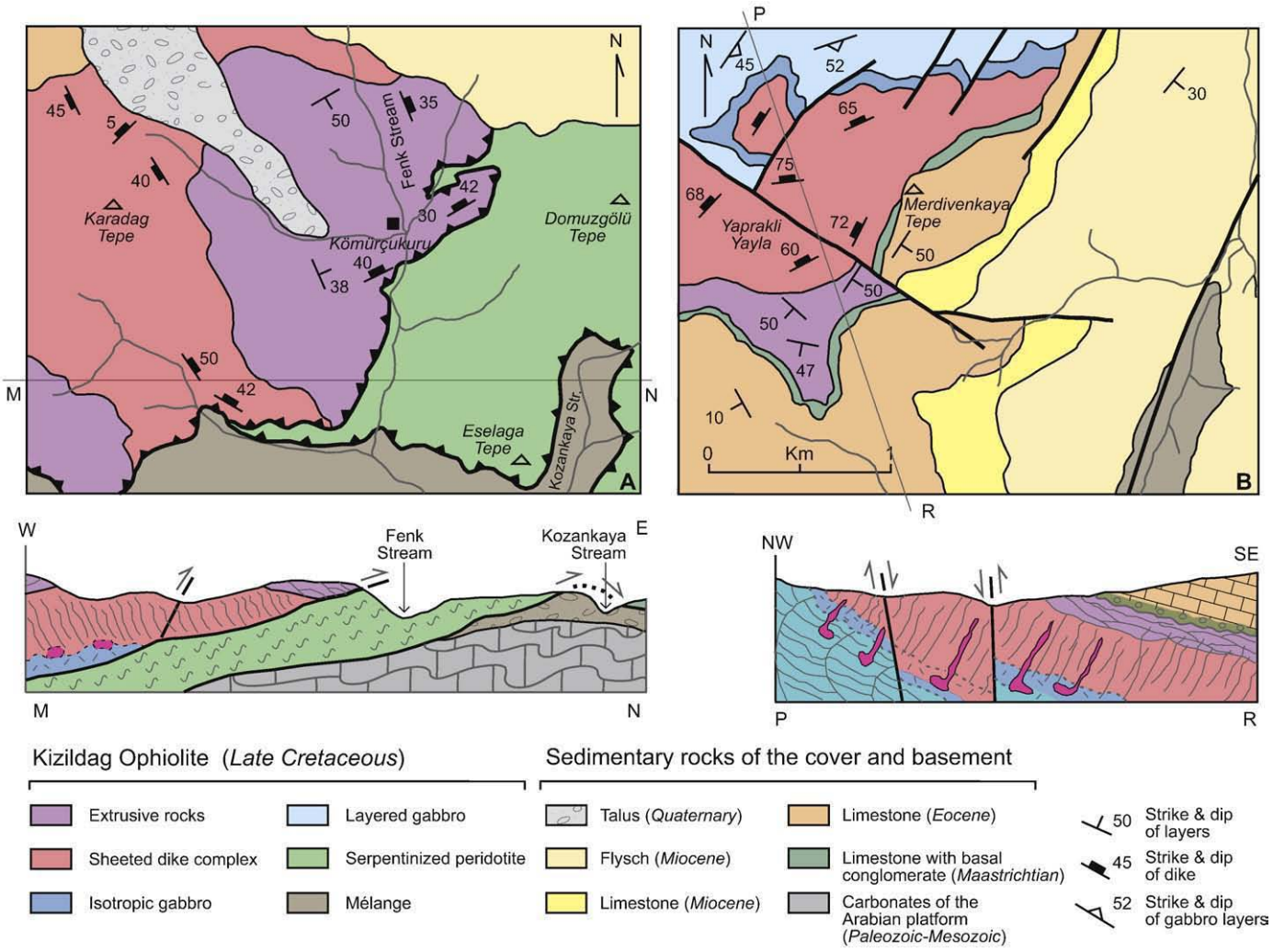

Fig. 5. A. Kizildag ophiolite, affected by emplacement-related contractional deformation is in thrust contact with the underlying ophiolitic mélange and the Aptian–Albian shelf carbonates of the Arabian platform. B. Crustal units of the Kizildag ophiolite are unconformably overlain by the post-emplacement sedimentary cover, including, from bottom to top, a Maastrichtian limestone with a basal conglomerate, a Paleocene–Eocene limestone, and a Miocene limestone–flysch sequence.

tectonically advancing Kizildag–Baër-Bassit ophiolite nappe, and resembles other well-documented mélanges associated with the Cretaceous Tethyan ophiolites in the Tauride belt (Polat et al., 1996; Dilek et al., 1999; Robertson, 2002).

4. Petrology

Coarse to medium-grained, predominantly lherzolitic to harzburgitic peridotites constitute the main lithological component of the ophiolite (Çogulu et al., 1975; Piskin et al., 1990; Dilek and Thy, 1998). The peridotites vary from massive to layered with banding caused by segregation of pyroxenitic and dunitic layers (Piskin et al., 1990). Dikes and pods of dunite and chromitite bodies are also found throughout the peridotite massif (Fig. 6I). Serpentinization is pervasive and commonly obscures the primary igneous mineralogy and metamorphic structures in these ultramafic rocks. The mineral chemistry of the Kizildag peridotites is typical for refractory and depleted mantle rocks with olivine (Fo_{92}), orthopyroxene (Mg# 0.92), clinopyroxene (Mg# 0.91), and chromian spinel (Piskin et al., 1990). Pegmatitic gabbroic (An_{91-95}) and pyroxenitic dike bodies occur principally toward the upper part of the peridotite and at the peridotite-cumulate boundary (Çogulu, 1980; Tinkler et al., 1981; Erendil, 1984; Tekeli and Erendil, 1986). These coarse-grained intrusives are distinctly more evolved than their host peridotites (Piskin et al., 1990).

Coarse- to medium-grained, layered and laminated gabbros and ultramafic rocks overlie the peridotite massif (Fig. 6F, H) and are composed dominantly of olivine gabbros, gabbronorites, and wehrlites. Bagci et al. (2005) infer the primary crystallization order in these rocks to have been olivine, clinopyroxene, plagioclase, orthopyroxene. Plastic deformation bands and crosscutting intrusive contacts suggest that these cumulate rocks underwent multiple stages of synmagmatic extension and crustal accretion. The wehrlites and gabbros are typical cumulates (Irvine, 1982) with lamination and layering as the predominant structures and are texturally dominated by adcumulates (Wager et al., 1960). The compositions of the coexisting plagioclase and clinopyroxene phases in these cumulates are shown in Fig. 7 as anorthite-content of plagioclase (An mol%) against Mg/(Mg + Fe*) ratio of clinopyroxene (Mg# with Fe* being total iron). The Kizildag cumulates, despite similar Mg#'s of their clinopyroxene, lack the very calcic plagioclase that is found in the Troodos ophiolite (Thy, 1987; Hébert and Laurent, 1990; Bagci et al., 2005); this character of the Troodos cumulates has been interpreted as sodium depletion and/or high water content of the parental magma (Thy, 1987; Sobolev et al., 1993; Panjasawatwong et al., 1995). Toward the overlying sheeted dike complex, the layered gabbros in Kizildag grade into isotropic gabbros and diorites, which have plagioclase compositions of An_{70} with the coexisting pyroxenes replaced by actinolite (Piskin et al., 1990).

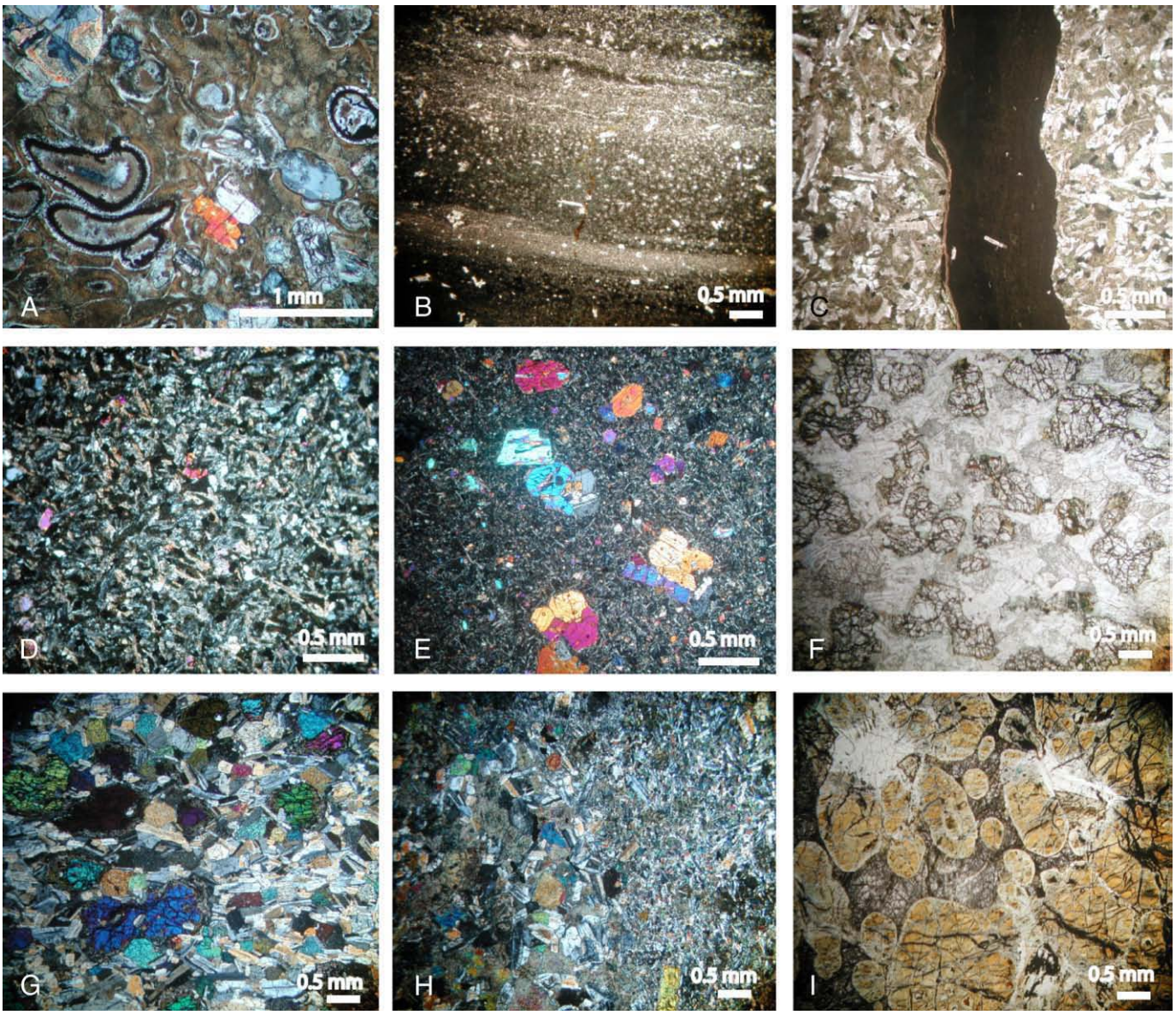

Fig. 6. Microphotographs to illustrate typical rock textures and mineralogy. A. Hyaloclastite with phenocrysts of plagioclase and clinopyroxene and filled vesicles (97-KD-3, Tahtaköprü Village). Excess blue coloration is due to the use of a blue dyed epoxy. B. Basaltic dikelet from near Ikizköprü (97-KD-22) showing alteration and chilled-margin effects against a medium-grained dolerite dike (bottom of the image). C. Medium-grained dolerite dike crosscut by a 2-mm-thick basaltic dikelet from the Arsuz road near Çevlik (97-KD-45). D. Dike intruding sheeted dikes from the Arsuz road near Çevlik (97-KD-34). E. Evolved mildly augite–plagioclase-phyric dike from the Arsuz road near Çevlik (97-KD-36). F. Mafic band in a layered olivine gabbro from the Arsuz road near Çevlik (97-KD-49). G. Laminated olivine gabbro from the Arsuz road near Çevlik (97-KD-47). H. Grain-size banding in gabbro from the Çevlik–Arsuz road (97-KD-51). I. Dunite dike in a serpentinized peridotite near the town of Deliler (97-KD-04).

Undeformed medium- to fine-grained discordant basaltic dikes and intrusive sills (Fig. 6B, C) occur within the peridotite and at the peridotite-cumulate gabbro contact as well as in the layered cumulate section (Piskin et al., 1990; Dilek and Thy, 1998). These dikes and sills are typically made of fine- to medium-grained, aphyric basalt with rare augite and plagioclase phenocrysts (Fig. 6D). Alteration to rodingites and amphibolites are pervasive in these dike rocks (Çogulu, 1980) and commonly obliterates the primary mineralogy and textures that appear to be similar to those in the sheeted dike complex as well as in the plutonic intrusives in the peridotite section. Mildly clinopyroxene–plagioclase-phyric dikes locally occur in the peridotites showing examples of skeletal pyroxene growth forms (Fig. 6E).

The majority of the sheeted dikes that make up the first dike generation are petrographically similar to the intrusive bodies found lower in the igneous stratigraphy. These sheeted dikes have fine-grained chilled margins and medium-grained centers (Erendil, 1984; Dilek and Delaloye, 1992). Dike rocks are aphyric to massive with locally occurring plagioclase and augite microphenocrysts in subophitic to interstitial primary textures. All these original igneous features are pervasively altered due to hydrothermal activities and the primary minerals have been metamorphosed to albite and actinolite with augite only present as relict grains surrounded by actinolite. The metamorphic grade increases with increasing depth in the sheeted dike complex from actinolite–chlorite (350–450 °C) to actinolite–epidote (475–550 °C) assemblages (Erendil, 1984; Lytwyn and Casey, 1993).

Pillow lavas and massive sheet flows together with minor hyaloclastites (Fig. 6A) constitute the main component of the Kizildag extrusive sequence (Dilek et al., 1991; Dilek and Delaloye, 1992). Hyaloclastites and pillow lavas are vesicular and aphyric with plagioclase and pyroxene microphenocrysts in a fine-grained groundmass. Hydrothermal alteration and vesicle fillings are common in the lavas. The sakalavites described by Dubertret (1955) and Laurent et al. (1980) contain olivine (Fo_{76}) and plagioclase (An_{87}) phyric basalts with a glassy groundmass. Analyses of the glassy sakalavite lavas indicate a depleted basalt composition similar

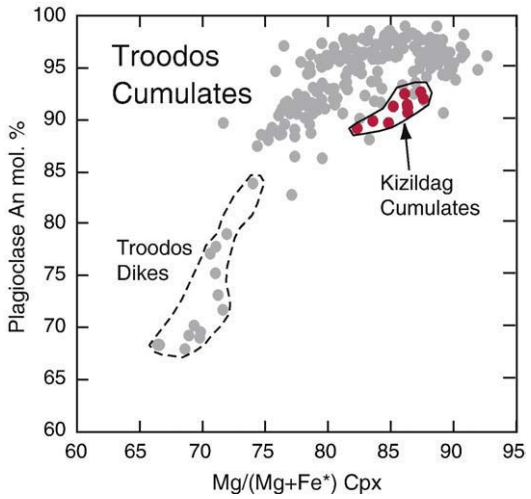

Fig. 7. Coexisting plagioclase (An mol%) and clinopyroxene [Mg/(Mg + Fe*)] of Kizildag cumulates (Bagci et al., 2005) compared to the Troodos ophiolite (Thy et al., 1989).

to comparable basalt glasses found in the UPL series of the Troodos complex (Robinson et al., 1983; Thy and Xenophontos, 1991).

5. Geochemistry

One of the principal goals of this study is to identify among the Kizildag lavas and dikes the magma groups that allow a direct compositional comparison to the dikes and extrusive suites of the Troodos and possibly the Baër-Bassit (Syria) ophiolites. Earlier work by Dubertret (1955) and Laurent et al. (1980) has suggested that boninitic types of magmas exist among the dominantly island arc tholeiites of the Kizildag extrusives (Dilek and Thy, 1998). The clear identification of such magma types in Kizildag, particularly if based on trace element characteristics, would be valuable for allowing a better correlation among these three ophiolites that are spatially close (Fig. 1) in the eastern Mediterranean region.

5.1. Analytical techniques

About 50 representative samples of Kizildag pillow lavas, dikes, and gabbros were investigated as part of this and our earlier study (Dilek and Thy, 1998). The major elements were analyzed by X-ray fluorescence (XRF) as detailed by Johnson et al. (1999) reporting all iron as FeO. The trace elements were either analyzed by XRF on low dilution Li-tetraborate fused tablets (Johnson et al., 1999) or by inductively-coupled plasma mass-spectrometry (ICP-MS) using standard acid digestion techniques (Crock and Lichte, 1982). The analytical precision (measured as the standard deviation of replicate analyses) is for the major oxides typically 0.03–0.05 wt.% and 1–2 ppm for the trace elements (XRF). The precision of the ICP-MS trace element analyses are mostly well below 1 ppm. Our analytical results are presented in Table 2 and are supplemented in this study with some data from Lytwyn and Casey (1993) for dikes and lavas, Laurent et al. (1980) for the sakalavite lavas, and Bagci et al. (2005) for wehrlites and gabbros. The pillow lavas described by Dubertret (1955) as sakalavites are included among the lavas and dikes discussed and analyzed as part of this study. Other analytical data relevant to this study can be found in Çogulu et al. (1975), Delaloye et al. (1979), Erendil (1984), Delaloye and Wagner (1984), and Piskin et al. (1990).

5.2. Major and trace element geochemistry

The analyzed basaltic dikes and lavas are mostly hypersthene- and olivine- to quartz-normative, subalkalic basalts, basaltic andesites, and andesites with SiO_2 up to 59 wt.% (Fig. 8) and Mg/(Mg + Fe*) ratios between 0.80 and 0.55. A group of mostly dikes and some lavas are made of highly quartz-normative dacites and rhyolites with Mg/(Mg + Fe*) ratios below 0.50. The major elements display large compositional variations in normative and major oxide compositions reflecting in part extensive low-grade, hydrothermal metamorphism (Çogulu, 1980; Erendil, 1984; Lytwyn and Casey, 1993). This strong alteration effect in the Kizildag ophiolite makes the identification of parental magma groups difficult and restricts the usefulness of the major element compositions. However, the large variation in normative compositions at a constant SiO_2 content in Fig. 8 cannot be attributed alone to alteration because of a conspicuous lack of strong correlations between volatile content as measured by the loss-of-ignition (LOI) and elements easily modified by alteration (Na, Ca, Mg). The presence of the slightly nepheline- to highly olivine-normative compositions most pronounced for the pillow lavas (Fig. 8) is due to elevated Na_2O content attributable to alteration. It is thus believed that the primary magmas for the Kizildag dikes and lavas reflect multiple parental magmas, as also suggested by Bagci et al. (2005) based on the gabbro mineralogy. The parental magmas likely varied from slightly olivine- to strongly quartz-normative compositions. This inference is in contrast to the observations of Thy and Xenophontos (1991) from the Troodos ophiolite, suggesting that the glassy Troodos lavas were entirely hypersthene–quartz normative.

The most pristine and primitive Kizildag lavas and dikes are highly magnesian with well above 8 wt.% MgO, 9.1–11.8 wt.% CaO, and very low Na_2O content of 1.0–1.5 wt.% Na_2O (Fig. 9). These samples are from a group of consistently quartz-normative rocks well characterized by lava flows described as glass-bearing by Laurent et al. (1980) and referred to as sakalavites following earlier work by Dubertret (1955). These latter flows also show restricted SiO_2 (52.2–54.9), TiO_2 (0.35–0.38), and Al_2O_3 (14.3–15.1) contents (Fig. 9). The SiO_2 content of the relatively unaltered basaltic dike and lava flows (50–57 wt.%) is systematically high compared to oceanic basalts with similar MgO contents (>6 MgO wt.%) (Dilek and Thy, 1998). A small group of analyzed silicic dikes in Kizildag (second generation dikes) are similar to other island arc andesites, dacites, and rhyolites with SiO_2 well above 57 wt.% (Dilek et al., 2008, and references therein).

Laurent et al. (1980) and Dilek and Thy (1998) have pointed out earlier that some of the basaltic Kizildag dikes (third generation dikes in this study) and lava flows show strong similarities to the boninites of the Troodos ophiolite by having elevated SiO_2 and Al_2O_3, and suppressed TiO_2, FeO, and P_2O_5 (all relatively to similar MgO contents). The evidence from the alkali elements is more ambiguous due to alteration effects. Nevertheless, the strong depletion in Na_2O and K_2O

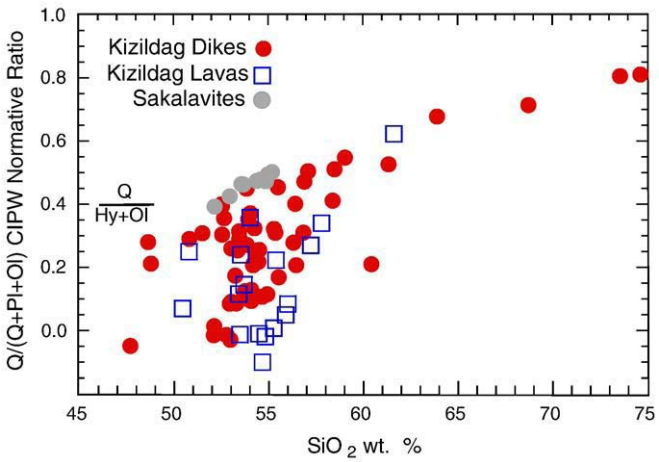

Fig. 8. Normative compositions [Q/(Q + Pl + Ol)] as a function of SiO_2 content (wt.%). The normative ratio is the CIPW molecular norm with the ferric/ferrous iron ratio adjusted to the fayalite–magnetite–quartz oxygen buffer (Kilinç et al., 1983). Normative nepheline is shown as negative normative ratios. The appearance of normative quartz is at a Q/(Q + Pl + Ol) ratio of 0.4.

observed for some relatively unaltered dikes and lava flows in Kizildag confirm the similarities to the Troodos boninites (Robinson et al., 1983; Thy and Xenophontos, 1991) for at least part of the Kizildag suite. The lack of strong FeO and TiO_2 enrichment further confirms the island arc affinity of the majority of the Kizildag suite (Fig. 9). Although we can only infer the stratigraphic position of the Kizildag boninitic lavas based on a circumstantial biostratigraphic correlation, it is highly likely that they represent the latest extrusives in the ophiolite, whereas the silicic arc-type lavas represent the relatively older extrusives in a lower stratigraphic position, as is the case for the Troodos suites (Thy and Esbensen, 1993; Dilek and Flower, 2003).

Fig. 9 illustrates the detailed major oxide relations of the Kizildag volcanic and plutonic rocks in comparison to the lavas and dikes of the Troodos and Baër-Bassit ophiolites. The Kizildag suite is characterized by a negative correlation between SiO_2 and FeO* (iron calculated as total FeO) for both pillow lavas and dikes without any indication of an early iron enrichment (Fig. 9A). The TiO_2 content slightly increases with decreasing MgO, paralleling a similar trend seen for the Troodos volcanics at only slightly higher concentrations (Fig. 9B). The majority of the Kizildag volcanics plot near or within the boninitic UPL field of the Troodos extrusive sequence. The Baër-Bassit ophiolite contains basaltic extrusives (Al-Riyami et al., 2002) similar in composition to those found among the Kizildag and Troodos lavas (Fig. 9).

The systematic high Al_2O_3 content of the majority of the basaltic Kizildag rocks, when compared to oceanic basalt compositions (Iceland; Fig. 9C), does not support extensive early low-pressure, plagioclase fractionation that would have resulted in strong depletion in Al_2O_3, as seen for the Iceland field. The relatively high Al_2O_3 content for basaltic rocks with MgO contents above 6 wt.% is, therefore, likely a primary feature inherited from liquids in equilibrium with the mantle peridotites. Melting experiments on peridotites have suggested that high SiO_2 and low FeO and MgO melts may result from low-pressure melting (Niu and Batiza, 1991; Langmuir et al. 1992; Takahashi et al., 1993). Low melt fractions are not supported by the relatively low concentrations of TiO_2 as well as of many trace elements. The Al_2O_3 enrichment may also in part be caused by hydrous fractionation (or melting) that can suppress plagioclase saturation (Asimow et al., 2004). The widespread presence of wehrlites among the Kizildag cumulate rocks (Piskin et al., 1990; Bagci et al., 2005) supports the idea of an early fractionation of olivine and clinopyroxene and a relatively late introduction of plagioclase producing gabbroic cumulates (Bagci et al., 2005). As illustrated in Fig. 9A, the fractionation of wehrlite drives melt compositions toward iron depletion and silica enrichment in contrast to the gabbro fractionation that results in iron enrichment. This observation parallels that from the Troodos ophiolite, for which a late introduction of plagioclase can also be documented (Thy et al., 1989; Thy and Xenophontos, 1991).

Trace element concentrations, in particular the rare earth elements, can be used to identify magma groups and the nature of the peridotite source, which produced the Kizildag volcanics. The rare earth element (REE) concentrations are shown in Fig. 10 normalized to CI chondrite (Sun and McDonough, 1989). These show similar depleted patterns for the light rare earth elements (LREE) compared to the heavy rare earth elements (HREE) (Fig. 10A). The Kizildag dikes have mostly low La/Sm_N ratios (0.5–1.0, normalized to chondrite), whereas the Dy/Yb_N ratios are just above unity (1.1–1.2). In addition, the LREE show consistently slight upturned La–Pr profiles that were also identified by Taylor and Nesbitt (1988) for the Troodos lavas (Type II).

A small group of Kizildag dikes shows strong enrichment in the LREE (La–Nd) and is composed of andesites or dacites (Fig. 5A; 94KD17, 94KD22). Another group of dikes is characterized by a very strong depletion in both LREE and HREE (94KD11, 97KD14, 97KD62). This latter group shows strong similarities to the strongly depleted boninitic lavas of the Troodos ophiolite with marked upturns for the most light REE (Type III lavas; Cameron, 1985; Taylor and Nesbitt, 1988). Because of the extensive hydrothermal alteration of the Kizildag lavas, only five reliable analyses were available (Fig. 10B), which closely parallel our observations for the dikes. One of the analyzed lavas (97KD07) shows the same general strong depletion also seen for the dikes with relatively depleted LREE and an upturn in La–Pr. The remaining four analyzed lavas are similar to the dominant dike group. This suggests that we can identify strongly depleted dikes and lavas in the Kizildag ophiolite that are similar in terms of REE to the UPL of the Troodos ophiolite (Fig. 10C; boninites or Types II and III lavas; Cameron, 1985; Taylor and Nesbitt, 1988), and the boninites from the Western Pacific (Crawford et al., 1981, 1989). It is not possible to identify similar REE pattern in the data available for the Baër-Bassit ophiolite, although Al-Riyami et al. (2002) have argued that minor and trace elements show strongly depleted characteristics similar to the Troodos boninites.

All analyzed Kizildag basaltic dikes and lavas are markedly depleted in both high-field strength (HFS) and heavy rare earth (HRE) elements compared to normal MORB (Fig. 11A, B). The boninitic dikes and lavas show an enhanced depletion in most HFSE in addition to the HREE (Fig. 11A, B), as also seen for the Troodos (Rautenschlein et al., 1985; Cameron, 1985; Taylor and Nesbitt, 1988). The large-ion lithophile (LILE) (Ba, Rb, K, and Sr) elements show strong enrichments that may be attributed to alteration effects. The cumulate gabbros are clearly distinguished from the dikes and lavas on the trace element diagrams by their depletion in most incompatible elements and characteristic 'saw-blade' trace element patterns (Figs. 10B and 11B).

6. Petrogenesis and tectonomagmatic evolution

The present results document that many of the absolute and relative trace element concentrations of the Kizildag ophiolite show strong similarities to those of the extrusive rocks in the Troodos ophiolite. Both ophiolites have low incompatible trace element concentrations and are strongly depleted in the LREE in particular. There appear to be two groups of basaltic dikes based on their geochemical characteristics: a relatively low La/Sm_N group (0.5–0.7) with low MgO (7–9 wt.%) and high TiO_2 (0.7–1.0 wt.%), and a high La/Sm_N group (0.8–1.0) with high MgO (9–11 wt.%) and low-TiO_2 (0.3–0.4 wt.%). The low La/Sm_N group also tends to exhibit high Dy/Yb_N ratios. Modeling of absolute and relative REE and HFSE concentrations suggests that aggregated fractional melting models using a fertile spinel lherzolite source (low to intermediate pressure) fail to reproduce the observed low-Ti contents and high La/Sm_N ratios for the Kizildag boninites making up the second group (Dilek and Thy, 1998). Better correspondences between the observed and modeled results can be achieved by assuming a small prior depletion (1–3%) of the source. Both the island arc tholeiites (first group) and the boninites (second group) in Kizildag record high extent of melting, although the boninites reflect the highest extent of melting and also show the least depletion in the LREE (highest La/Sm_N ratios). This 'positive' correlation between the extent of melting and the LREE enrichment can be related to source metasomatic transformation and modifications, and their effects on melting (Taylor and Nesbitt, 1988).

Modeling of high extent of melting (~20%) has shown that melts extracted from a depleted mantle source and enriched by small amounts of fluid released from a subducting oceanic slab can explain the main features of the trace element characteristics of the Kizildag rocks (Dilek and Thy, 1998). The most refractory liquids (boninitic) are related to an enriched source, while the least refractory liquids (island arc tholeiites) record little or no enrichments. The nature of the enriching fluid or liquid is uncertain (Tatsumi et al., 1986; Taylor and Nesbitt, 1988; Pearce and Parkinson, 1993; Stolper and Newman, 1994; Cousens et al., 1994) and thus permits a high degree of freedom in the model development.

The Troodos ophiolite shows many similarities to the Kizildag ophiolite both in terms of major and trace element variations. Both ophiolites show signs of progressive melting of a variably depleted source (Cameron, 1985; Lytwyn and Casey, 1993). Slightly to marked U-shaped LREE patterns are most strongly developed by highly refractory melts of the Troodos ophiolite (Types II and III of Cameron, 1985), but

Table 2
Major and trace element compositions of representative dikes, gabbros, and extrusive rocks, Kizildag ophiolite in Turkey.

Major elements (XRF, wt.%)

Sample	SiO_2	TiO_2	Al_2O_3	FeO	MnO	MgO	CaO	Na_2O	K_2O	P_2O_5	Total
97KD-07	48.97	0.49	17.57	9.70	0.17	6.05	10.64	2.50	0.08	0.04	96.22
97KD-09	51.35	0.35	15.96	8.19	0.29	6.00	10.04	3.49	0.08	0.03	95.78
97KD-14	51.82	0.36	13.30	7.83	0.16	10.97	12.02	1.64	0.19	0.03	98.32
97KD-24	51.03	0.39	15.47	7.62	0.14	10.62	9.74	2.04	0.38	0.04	97.47
97KD-25	63.34	0.89	15.04	6.37	0.05	4.35	5.34	2.62	0.95	0.09	99.04
97KD-26	55.55	0.82	15.59	5.77	0.07	8.56	7.30	4.58	0.24	0.06	98.53
97KD-32	52.49	0.74	15.86	8.01	0.14	8.24	9.15	2.89	0.51	0.06	98.09
97KD-33	53.92	0.71	16.50	6.87	0.10	7.39	9.58	3.99	0.29	0.06	99.41
97KD-34	52.03	0.48	15.59	7.40	0.13	8.87	9.27	4.06	0.12	0.04	97.99
97KD-35	74.32	0.62	12.13	3.30	0.02	1.16	2.41	5.17	0.28	0.10	99.51
97KD-38	51.01	0.80	16.16	9.41	0.07	8.54	8.55	1.85	0.50	0.05	96.94
97KD-44	51.70	0.60	15.67	7.82	0.15	7.58	9.46	3.71	0.24	0.05	96.98
97KD-45	52.21	0.93	15.31	8.66	0.16	7.10	9.48	3.55	0.22	0.07	97.69
97KD-50	52.64	0.74	16.28	8.14	0.19	8.69	6.87	2.80	0.87	0.07	97.29
97KD-61	51.76	0.49	16.57	7.18	0.12	8.33	11.37	2.36	0.17	0.04	98.39
97KD-62	51.07	0.33	12.76	7.52	0.12	14.09	10.09	1.03	0.09	0.03	97.13
97KD-69	53.97	0.58	16.23	6.78	0.13	4.95	11.37	4.80	0.05	0.05	98.91
94KD-02	54.01	0.40	16.13	7.44	0.15	7.17	6.15	6.96	0.19	0.03	98.62
94KD-08	49.20	0.32	17.57	5.98	0.13	10.12	12.75	2.26	0.28	0.03	98.64
94KD-11	52.82	0.74	15.96	9.39	0.14	8.71	6.82	3.73	0.18	0.06	98.55
94KD-12	53.53	0.95	15.57	8.95	0.12	7.28	6.75	4.60	0.32	0.08	98.15
94KD-17	57.98	1.06	15.91	7.68	0.06	6.09	5.03	5.00	0.30	0.08	99.20
94KD-20	52.37	0.42	15.98	5.27	0.11	10.09	12.22	3.16	0.18	0.04	99.85
94KD-22	53.02	0.68	15.74	8.05	0.15	7.69	7.36	4.84	0.27	0.07	97.87
94KD-23	52.36	0.37	13.19	8.06	0.15	11.23	8.49	4.12	0.11	0.03	98.11
94KD-24	48.40	0.23	7.10	10.40	0.16	19.96	10.46	0.60	0.15	0.02	97.47
94KD-25	51.04	0.31	15.93	6.05	0.12	10.76	14.23	1.57	0.08	0.03	100.12
94KD-27	68.84	0.74	13.56	5.35	0.03	2.51	3.24	5.21	0.40	0.20	100.08

Trace elements (XRF, ppm)

Sample	Ni	Cr	Rb	Zr	Sr	Y	Sc	Ba	V	Nb	Ga	Cu	Zn
97KD-07	43	46	1	34	325	18	42	31	312	2	18	85	78
97KD-09	73	162	3	18	24	11	40	16	276	1	23	11	42
97KD-14	134	813	1	22	138	12	41	41	235	1	9	2	35
97KD-24	103	307	4	25	156	12	33	9	214	2	15	2	26
97KD-25	25	10	5	74	132	34	20	nd	213	4	18	1	5
97KD-26	33	28	2	43	147	27	29	17	368	3	15	nd	7
97KD-32	57	75	3	39	115	19	33	17	258	2	15	13	23
97KD-33	42	51	1	38	105	20	33	44	269	3	16	10	11
97KD-34	80	247	1	25	42	13	30	3	248	3	16	92	50
97KD-35	13	8	3	106	121	36	6	21	93	8	13	3	1
97KD-38	42	84	2	37	104	18	31	7	283	2	18	nd	4
97KD-44	53	75	1	32	128	15	33	16	223	2	16	5	36
97KD-45	53	111	1	48	106	22	32	21	259	2	14	13	21
97KD-50	43	60	5	41	77	19	34	20	256	2	17	60	105
97KD-61	78	183	nd	27	71	15	33	14	253	2	13	1	11
97KD-62	308	861	nd	16	39	9	31	8	207	2	13	5	31
97KD-69	43	115	1	31	58	16	36	4	260	2	18	9	48
94KD-02	58	81	3	24	67	11	32	nd	215	4	9	130	53
94KD-08	113	463	1	18	130	10	49	nd	206	3	14	32	24
94KD-11	34	42	2	36	97	19	35	nd	270	4	19	11	32
94KD-12	32	16	2	48	116	23	35	12	279	3	12	3	14
94KD-17	30	48	1	59	117	23	32	1	351	8	18	2	6
94KD-20	121	399	1	27	88	14	45	nd	211	1	11	11	26
94KD-22	80	203	2	83	326	17	20	nd	245	12	14	32	41
94KD-23	213	633	1	20	79	11	38	nd	230	1	12	100	57
94KD-24	535	1637	1	13	47	8	41	nd	169	1	9	14	45
94KD-25	168	598	2	22	74	10	42	nd	165	2	14	88	34
94KD-27	19	19	3	95	113	23	17	nd	155	3	14	2	5

Rare earth elements (ICP-MS, ppm)

Sample	La	Ce	Pr	Nd	Sm	Eu	Gd	Tb	Dy	Ho	Er	Tm	Yb	Lu
97KD-07	1.02	2.4	0.42	2.6	1.2	0.48	2.1	0.41	3.0	0.7	2.0	0.3	1.9	0.30
97KD-09	0.67	1.2	0.19	1.1	0.6	0.27	1.1	0.23	1.8	0.41	1.2	0.19	1.3	0.20
97KD-14	0.52	1.1	0.19	1.2	0.6	0.23	1.2	0.26	2.0	0.45	1.3	0.20	1.4	0.22
97KD-24	0.78	1.9	0.32	1.8	0.9	0.40	1.5	0.30	2.1	0.47	1.4	0.2	1.3	0.20
97KD-25	3.1	7.7	1.2	7.0	3.0	1.0	4.5	0.9	6.0	1.3	3.8	0.6	3.5	0.53
97KD-26	2.1	5.8	1.0	5.6	2.4	0.9	3.5	0.7	4.8	1.1	3.0	0.4	2.7	0.40
97KD-32	1.2	3.4	0.58	3.4	1.5	0.6	2.4	0.46	3.2	0.7	2.0	0.3	1.9	0.30
97KD-33	2.0	4.8	0.72	4.0	1.8	0.8	2.6	0.52	3.6	0.8	2.2	0.3	2.1	0.33
97KD-34	1.3	2.7	0.42	2.3	1.0	0.43	1.6	0.33	2.4	0.5	1.5	0.2	1.5	0.24
97KD-35	2.0	4.8	0.78	4.7	2.3	0.8	3.8	0.8	5.7	1.3	3.8	0.6	4.0	0.64
97KD-38	1.3	3.3	0.54	3.2	1.5	0.6	2.2	0.45	3.0	0.7	1.9	0.3	1.8	0.28
97KD-44	1.05	2.7	0.46	2.8	1.3	0.6	2.0	0.40	2.9	0.6	1.8	0.3	1.7	0.27

Table 2 (*continued*)

Rare earth elements (ICP-MS, ppm)

Sample	La	Ce	Pr	Nd	Sm	Eu	Gd	Tb	Dy	Ho	Er	Tm	Yb	Lu
97KD-45	2.0	5.4	0.88	5.1	2.1	0.9	3.1	0.6	4.1	0.9	2.5	0.4	2.2	0.36
97KD-50	1.6	4.0	0.65	3.7	1.7	0.7	2.5	0.48	3.4	0.7	2.1	0.3	2.0	0.31
97KD-61	1.7	3.1	0.46	2.5	1.1	0.5	1.9	0.40	2.7	0.6	1.7	0.3	1.6	0.26
97KD-62	0.35	0.79	0.15	1.0	0.6	0.24	1.0	0.22	1.6	0.37	1.1	0.17	1.1	0.17
97KD-69	1.4	3.1	0.49	2.9	1.3	0.54	2.0	0.39	2.8	0.6	1.8	0.3	1.7	0.28
94KD-02	1.09	2.1	0.30	1.5	0.7	0.33	1.2	0.26	1.8	0.41	1.2	0.18	1.2	0.19
94KD-08	0.79	1.2	0.28	1.2	0.6	0.33	1.1	0.22	1.6	0.36	1.0	0.14	0.9	0.15
94KD-11	1.4	3.2	0.56	3.2	1.5	0.6	2.3	0.46	3.2	0.7	2.1	0.3	1.9	0.30
94KD-12	1.7	4.4	0.77	4.4	2.0	0.8	3.0	0.6	4.0	0.9	2.5	0.4	2.3	0.36
94KD-17	4.2	7.5	0.9	4.5	1.9	0.7	2.8	0.6	3.8	0.9	2.5	0.4	2.4	0.39
94KD-20	1.3	2.7	0.49	2.4	1.1	0.51	1.8	0.38	2.4	0.6	1.6	0.2	1.5	0.23
94KD-22	8.9	14.1	1.5	5.9	1.7	0.7	2.2	0.43	2.9	0.6	1.8	0.3	1.7	0.28
94KD-23	1.03	1.7	0.31	1.4	0.7	0.30	1.3	0.27	1.9	0.46	1.4	0.2	1.3	0.22
94KD-24	0.59	0.80	0.20	0.8	0.44	0.20	0.8	0.15	1.1	0.26	0.7	0.11	0.7	0.10
94KD-25	1.04	1.7	0.37	1.6	0.7	0.34	1.2	0.26	1.8	0.39	1.1	0.16	1.1	0.16
94KD-27	1.7	3.9	0.61	3.5	1.6	0.7	2.6	0.50	3.5	0.8	2.3	0.3	2.2	0.36

Trace elements (ICP-MS, ppm)

Sample	Ba	Th	Nb	Y	Hf	Ta	U	Pb	Rb	Cs	Sr	Sc
97KD-07	30	0.20	2.0	19.1	0.71	0.2	0.10	0.9	1.6	0.03	341	55
97KD-09	5	0.13	1.3	11.1	0.44	0.09	0.08	0.8	3.2	0.06	22	52
97KD-14	23	0.15	1.5	11.8	0.49	0.1	0.07	0.14	1.2	0.10	138	49
97KD-24	9	0.10	0.55	12.7	0.55	0.04	0.04	0.19	2.0	0.02	149	45
97KD-25	11	0.6	2.5	36.1	2.3	0.2	0.2	0.6	3.6	0.03	134	29
97KD-26	15	0.23	1.2	27.8	1.2	0.08	0.10	0.21	1.2	0.02	146	43
97KD-32	9	0.13	0.8	19.5	1.0	0.05	0.06	0.48	2.3	0.02	111	41
97KD-33	47	0.19	1.0	21.3	1.1	0.08	0.1	0.31	1.8	0.02	102	42
97KD-34	4	0.16	1.1	14.2	0.70	0.08	0.07	0.54	0.41	0.02	40	42
97KD-35	28	1.3	5.0	37.6	3.6	0.4	0.4	0.24	1.2	0.02	117	12
97KD-38	5	0.16	0.9	17.3	0.9	0.07	0.07	0.13	2.4	0.02	93	38
97KD-44	14	0.12	0.7	16.5	0.8	0.06	0.05	0.16	1.1	nd	125	42
97KD-45	19	0.14	0.9	22.7	1.4	0.07	0.08	0.23	1.5	0.02	nd	39
97KD-50	22	0.18	1.0	19.2	1.1	0.07	0.08	1.0	4.3	0.06	75	39
97KD-61	11	0.20	0.8	15.5	0.72	0.07	0.06	0.10	1.0	nd	72	41
97KD-62	3	0.07	0.52	9.7	0.35	0.04	0.03	0.10	0.45	nd	35	38
97KD-69	6	0.16	1.0	16.0	0.8	0.07	0.09	0.7	0.36	nd	55	35
94KD-02	17	0.20	1.8	11.1	0.58	0.1	0.04	0.8	2.7	0.52	92	39
94KD-08	6	0.07	0.39	8.9	0.33	0.04	0.03	0.10	2.1	nd	124	44
94KD-11	14	0.15	0.9	18.4	1.0	0.07	0.06	0.15	1.2	nd	90	38
94KD-12	24	0.18	1.1	22.5	1.3	0.08	0.08	0.21	2.0	nd	111	36
94KD-17	8	1.0	5.1	22.6	1.6	0.4	0.2	0.19	2.2	nd	110	32
94KD-20	19	0.18	1.1	14.3	0.75	0.07	0.07	0.42	1.4	nd	85	40
94KD-22	31	2.0	10.4	17.1	1.7	0.7	0.6	0.6	1.8	nd	362	36
94KD-23	10	0.13	1.3	12.0	0.52	0.10	0.05	0.6	0.9	nd	80	42
94KD-24	4	0.06	0.32	6.5	0.22	0.02	0.02	0.24	0.9	nd	49	48
94KD-25	9	0.09	0.55	10.3	0.53	0.04	0.03	0.29	1.1	nd	76	44
94KD-27	9	0.3	2.4	21.8	3.1	0.2	0.2	0.19	1.9	nd	108	16

nd, not detected.

Kizildag ophiolite samples (36°E and 36°30′N):

97KD-07 Basaltic pillow lava.
97KD-09 Pillow lava crosscut by dike.
97KD-14 Dike intruding peridotite.
97KD-24 Microgabbro.
97KD-25 Dioritic dike intruding gabbro.
97KD-26 Basaltic dike crosscutting gabbro.
97KD-32 Sheeted dike.
97KD-33 Sheeted dike.
97KD-34 Sheeted dike.
97KD-35 Plagiogranite dike intruding sheeted dikes.
97KD-38 Sheeted dike.
97KD-44 Basaltic dike intruding sheeted dike complex.
97KD-45 Sheeted dike.
97KD-50 Pillow lava (sakalavite) overlying serpentinite.
97KD-61 Basaltic dike intruding isotropic gabbro.
97KD-62 Basaltic dike intruding gabbro.
97KD-69 Pillow lava.
94KD-02 Basaltic pillow lava.
94KD-08 Gabbro beneath the sheeted dike complex.
94KD-11 Sheeted dolerite dike.
94KD-12 Sheeted dolerite dike.
94KD-17 Doleritic dike intruding gabbro.
94KD-20 Gabbroic dike in the plutonic section.
94KD-22 Andesitic dike intruding layered gabbro.
94KD-24 Olivine gabbro of the plutonic section.
94KD-23 Gabbroic dike intruding gabbro.
94KD-25 Isotropic gabbro in the plutonic section.
94KD-27 Quartz andesite dike in the sheeted dike complex.

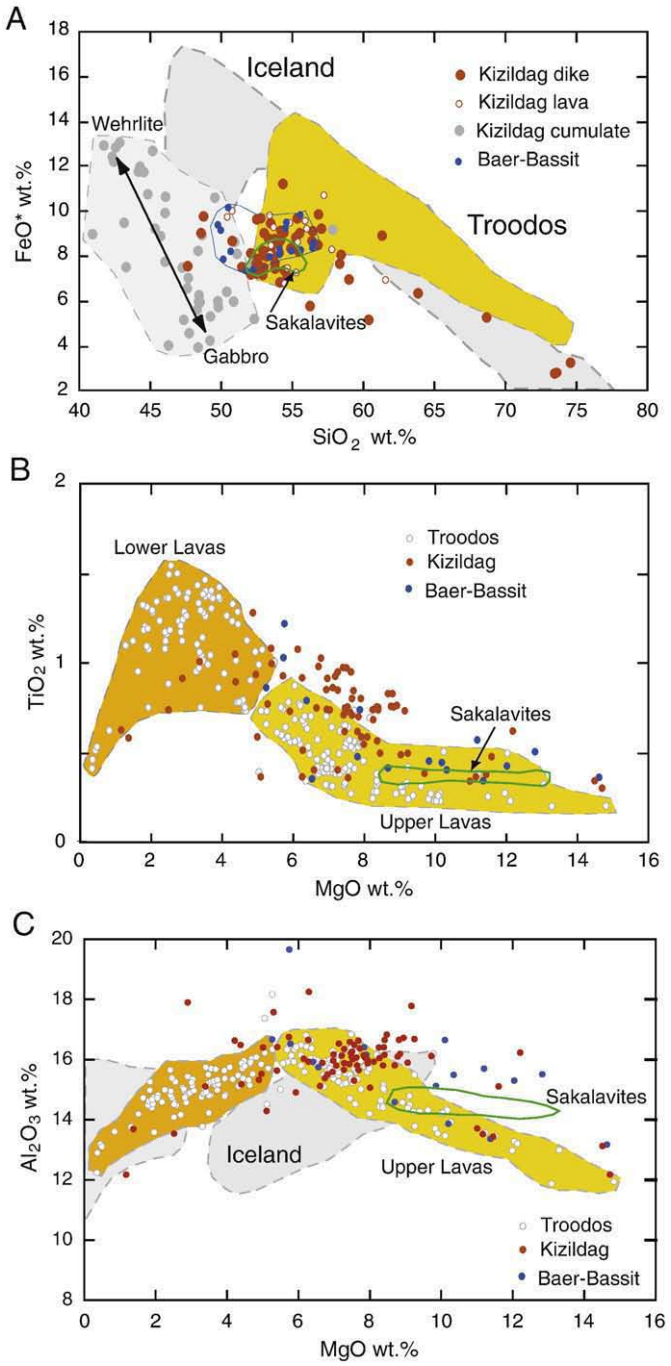

Fig. 9. Major element variations of the Kizildag volcanic, dike and plutonic rocks, and their comparisons to those of the Troodos and Baër-Bassit ophiolites. Source of the data: Kizildag rocks as of this study with additional data from Dilek and Thy (1998), Bagci et al. (2005), and Lytwyn and Casey (1993). Baër-Bassit lavas and dikes from Al-Riyami et al. (2002). Data for glass-rich sakalavite lavas in Kizildag from Laurent et al. (1990). Volcanic glass and dike analyses for the Troodos field from Thy and Xenophontos (1991) and Staudigel et al. (1999). The Iceland fields are based on analysis of volcanic glasses from various sources. A. FeO* as a function of SiO_2 wt.% (all iron is calculated as FeO). Wehrlite to gabbro cumulates are from Bagci et al. (2005). B. TiO_2 versus MgO wt.%. C. Al_2O_3 as a function of MgO wt.%. The Iceland glass compositions are outlined as two fields: a basaltic field with high MgO and a silicic field with low MgO.

also recorded by less refractory melts of both the Troodos and Kizildag ophiolites (Fig. 10). This characteristic LREE pattern can be related to metasomatic transformations of the source by an incompatible element-enriched, slab-derived component (McCulloch and Cameron, 1983; Cameron, 1985; Rautenschlein et al., 1985; Taylor and Nesbitt, 1988). Taylor and Nesbitt (1988) modeled the Troodos REE patterns and suggested an addition of only 0.2–0.3%-enriched liquids to a refractory liquid. The introduction of incompatible element-enriched fluid (or melt) may have facilitated enhanced degrees of melting or melting of relatively refractory mantle material (Taylor and Nesbitt, 1988).

We infer that the Kizildag ophiolite formed in a tectonic setting, where enriched fluids or melts were derived from deeper and more fertile sources, most likely a subducting slab, and where they were added to the overlying mantle or the mantle wedge (Fig. 12). Melting occurred at relatively low pressures within the stability field of spinel and proceeded to high melt fractions possibly by progressive depletion and melt removal. The subducting oceanic slab was a MORB-type lithosphere created earlier (Jurassic–early Cretaceous?) in the Southern Tethys, which had developed between the Tauride continental block (and its westerly continuation, Apulia) to the north and Afro-Arabia to the south (Fig. 12A). Following its inception, continued subduction and rapid rollback of the subducting slab generated IAT magmatism, producing a protoarc crust. Upper plate extension induced by slab rollback facilitated spreading within this protoarc environment, resulting in periodic replenishments of high-level open magma chambers and formation of the sheeted dike complex (inset in Fig. 12B).

The primary magmas were probably basaltic to basaltic andesitic in composition and were augmented by a continuous supply of undifferentiated magmas under these open-system conditions (Dilek et al., 1990; Beccaluva et al., 2004). This seafloor spreading stage of magmatism created much of the layered architecture (Penrose-type oceanic lithosphere, Dilek, 2003) of the Kizildag ophiolite, including the dunite, wehrlite, gabbro (layered and isotropic), sheeted dikes (first generation dolerite to second generation basaltic andesite and andesite dikes based on crosscutting relations), some plagiogranites, and pillow to massive lavas with basaltic to andesitic compositions. Later episodes of this stage of magmatism may have evolved toward relatively silicic compositions, producing more calc-alkaline rocks (Dilek et al., 1990).

The mantle flow facilitated by retrograde slab motion and the arc-wedge corner flow played a major role in the evolution of the melting column beneath the extending Kizildag protoarc to forearc. Furthermore, the influx of fertile mantle contributed additional material into upwelling mantle diapirs in the melting column (Fig. 12C). Highly enriched liquids from the lower fertile source mixed with variably refractory melts produced within this melting column, in which melt generation, aggregation and differentiation occurred in multiple levels (Dilek et al., 2008). Increased asthenospheric diapirism and rising temperatures in the subarc mantle and the mantle wedge may have triggered shallow partial melting of hydrous and refractory peridotites (Hickey and Frey, 1982; Cameron, 1985; Duncan and Green, 1987; Hickey-Vargas and Reagan, 1987; Crawford et al., 1989). This melting in turn produced further splitting of the nascent arc and very low-Ti tholeiites and boninitic magmas (Fig. 12C). These magmas formed andesitic, dacitic and boninitic dikes and lavas, and the late-stage crosscutting plutons that underplated the earlier-formed Kizildag oceanic lithosphere (inset in Fig. 12C. The magma chambers of this phase may have evolved in a relatively closed system with little or no replenishment, and chemical reactions and modifications in the plutonic and peridotite rocks may have occurred. Lherzolite, dunite, quartz–diorite and plagiogranite intrusions developed during this magmatic episode.

This multi-stage tectonomagmatic evolution of the Kizildag ophiolite was quite similar to that of the Troodos ophiolite, as envisioned by Dilek et al. (1990) and Lytwyn and Case (1993), and we infer that the coeval Baër-Bassit ophiolite had a similar evolutionary path. We do not think that these magmatic stages were separated significantly in time and space. Rather, we envision that the stages of IAT and boninitic magmatism overlapped and occurred closely in time (within <few m.y.) and space, as the crosscutting dike and volcano-stratigraphic relations both in Kizildag and Troodos show. The mantle

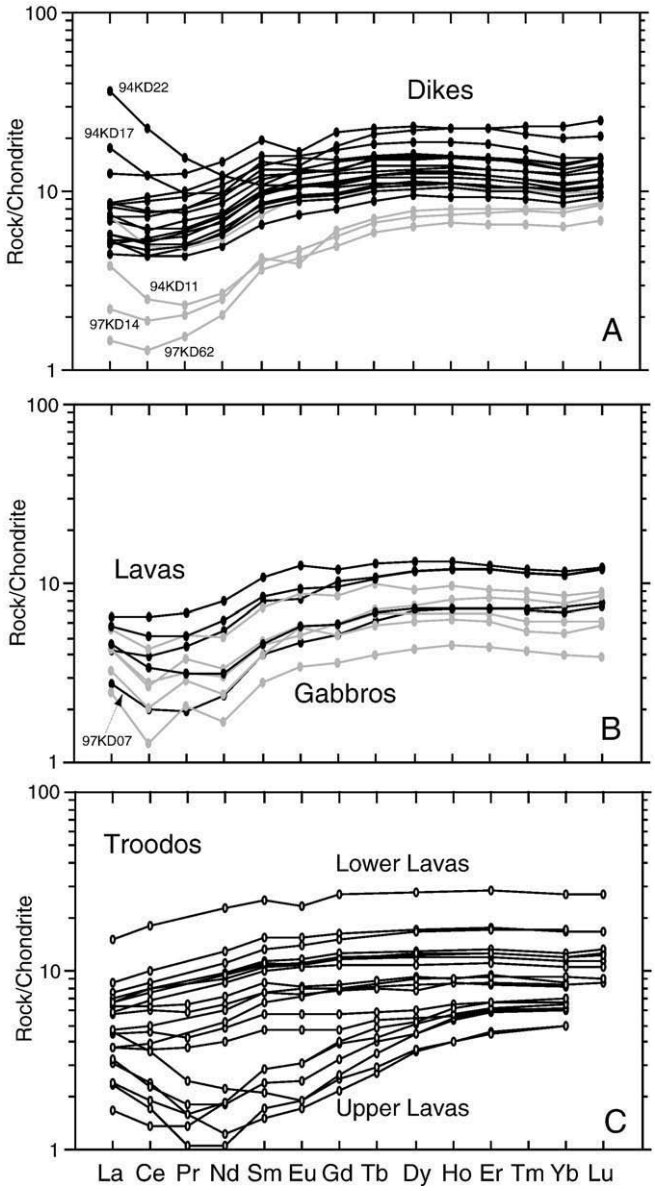

Fig. 10. Rare earth element concentrations of representative samples normalized to CI chondrite (Sun and McDonough, 1989). A. Dikes: andesitic dikes are marked 94KD-17 and 94KD-22. Strongly depleted dikes are 95KD11, 97KD14, and 97KD62. B. Lavas (black) and gabbros (gray shade). Strongly depleted sakalavite lava is 97KD07. C. Troodos dikes and lavas from Cameron (1985) and Rautenschlein et al. (1985).

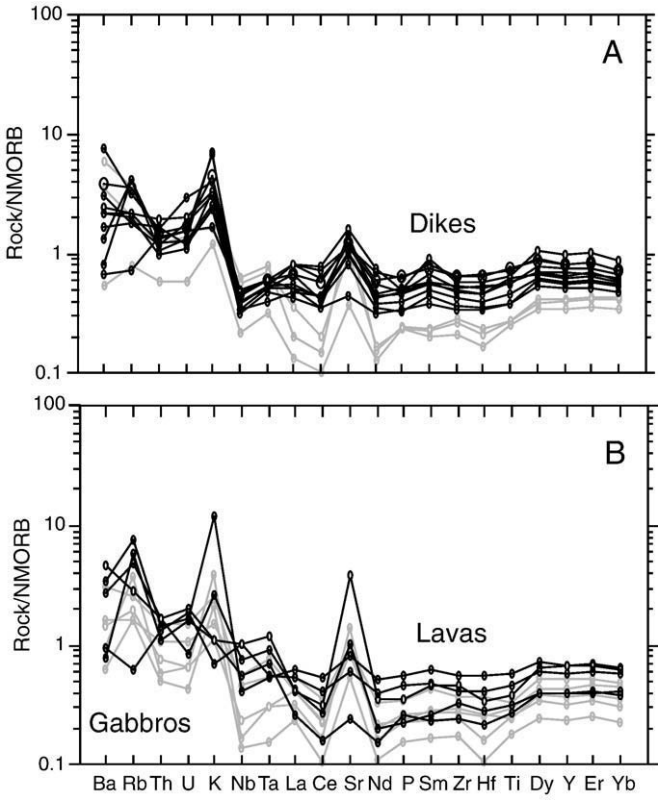

Fig. 11. Trace element compositions normalized to NMORB (Sun and McDonough, 1989). Selection of trace elements arranged in order of decreasing incompatibility. A. Dikes. B. Lavas (black) and gabbros (gray shade). The silicic dikes are not shown.

sources in both IAT and boninitic stages were depleted, although more or ultra-depleted in the latter case due to the repeated earlier melting episodes. Varying temperature conditions and water contents in the mantle wedge, both increased in the later boninitic stage, were responsible for producing these different magmatic series nearly contemporaneously. Similar observations and interpretations have also been made for the IAT and boninitic episodes of early arc volcanism in the Izu forearc region during the Eocene–Oligocene (Haraguchi and Ishii, 2007).

7. Conclusions

The Kizildag (Turkey), Baër-Bassit (Syria) and Troodos (Cyprus) ophiolites are coeval in age and represent the remnants of a ~92–90 Ma SSZ oceanic crust formed in Southern Tethys. All three ophiolites show a similar pseudostratigraphy, reminiscent of a Penrose-type oceanic crust with apparent layer-cake architecture. However, crosscutting relations of different dike generations and plutonic intrusions and the geochemical characteristics of these intrusive rocks and their volcanic counterparts indicate a multi-stage magmatic evolution of the ophiolites in an extended protoarc–forearc setting in a SSZ environment.

All analyzed sheeted dikes, extrusive rocks and gabbros in the Kizildag ophiolite show geochemical signatures of various degrees of melting of a variably depleted mantle source, which was metasomatized by incompatible element-enriched, slab-derived fluids. The majority of the sheeted dikes and extrusive rocks range in composition from basalt, basaltic andesite and andesite with IAT affinities. The late-stage dikes, gabbros, and lavas (sakalavites) with high MgO and low-TiO_2 contents and slightly to strongly U-shaped LREE patterns have boninitic compositions, indicating enhanced degrees of melting of highly refractory mantle peridotites. Crosscutting and overlapping relations of the intrusive and extrusive rocks show that these IAT to boninitic stages of magmatism developed very closely in space and time, nearly contemporaneously, during the evolution of the Kizildag ophiolite.

The IAT magmatism evolved from melting of subduction-modified mantle at low pressures within the stability field of spinel and proceeded to high melt fractions through progressive depletion and melt removal. Slab rollback-induced extension in the protoarc–forearc environment facilitated periodic replenishments of high-level open magma chambers by undifferentiated magmas. The arc-wedge corner flow and asthenospheric diapiric upwelling from more fertile sources at depth were instrumental in raising the temperatures in the melting column and triggering shallow partial melting of hydrous and refractory peridotites. The resulting boninitic magmas beneath the Kizildag forearc evolved in a relatively closed system with little or no

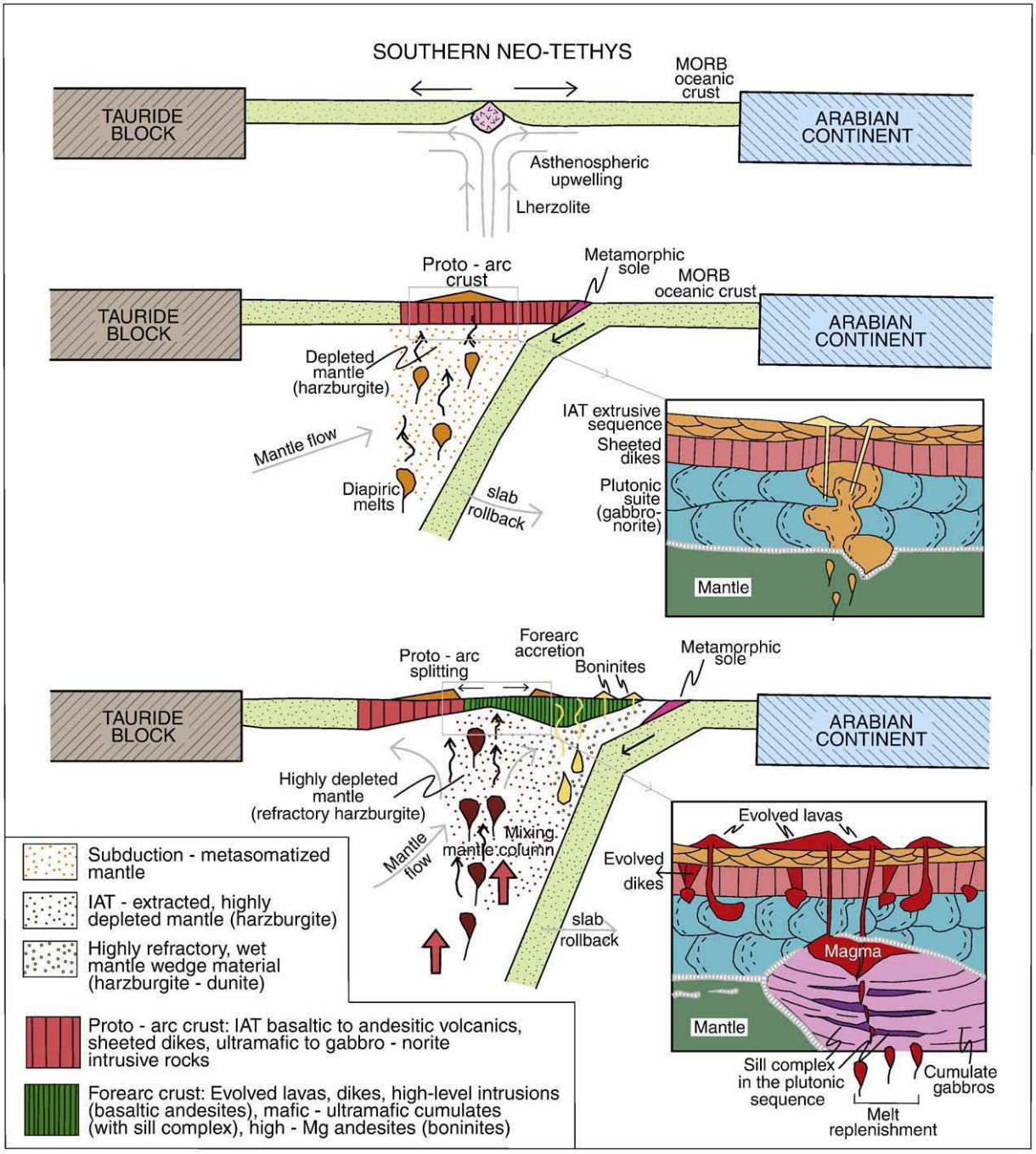

Fig. 12. Sequential geodynamic diagram depicting the tectonomagmatic evolution of the Kizildag ophiolite in an extended intra-oceanic arc–forearc SSZ setting between the Tauride and Arabian continental blocks in the late Cretaceous. The metamorphic sole shown in this diagram marks the inception of an intra-oceanic subduction zone in the Southern Neo-Tethys, as suggested for a likely mechanism for the formation of metamorphic soles in other ophiolites (Wakabayashi and Dilek, 2003), such as the Troodos (Chan et al., 2007), Baër-Bassit (Al-Riyami et al., 2002), and Oman (Hacker et al., 1996). See text for discussion.

replenishment, and their products underplated the earlier-formed IAT oceanic crust. Thus, the parental magmas of the Kizildag ophiolite evolved from variable mixing and differentiation of geochemically diverse melt increments in different levels within the melting column beneath the protoarc–forearc spreading system.

This evolutionary trend of the Kizildag ophiolitic magmas from IAT to boninitic affinities appears to be common in the evolutionary history of many Tethyan ophiolites and may reflect a blueprint of incipient arc magmatism in subduction zone factories. The nearly contemporaneous IAT to boninitic, early arc magmatism (Eocene–Oligocene) in the Izu–Bonin–Mariana system is the best modern analogue for the SSZ evolution of Tethyan ophiolites.

Acknowledgements

We thank Harald Furnes, Osman Parlak, Annie Rassios, Alastair Robertson, Paul Robinson, Emilio Saccani, and Minella Shallo for discussions on the geochemistry and tectonics of the Tethyan ophiolites, particularly those in Turkey, and Réjean Hébert and Paul T. Robinson for their thorough and constructive reviews of the paper for LITHOS. Support from the U.S. National Science Foundation, UNESCO Earth Sciences Division, and NATO (CRG-970263 and EST. CLG-97617) is gratefully acknowledged. We thank Barry Hanan at SDSU for zircon dating of our plagiogranite sample. We also thank Ömer Akinci and Ömer Elitok of the Süleyman Demirel University

(Isparta-Turkey) for their participation in fieldwork in Kizildag and the Governor of Hatay for his warm welcome and logistical help during our stay in and around the City of Hatay.

References

Al-Riyami, K., Robertson, A., Dixon, J., Xenophontos, C., 2002. Origin and emplacement of the Late Cretaceous Baër-Bassit ophiolite and its metamorphic sole in NW Syria. Lithos 65, 225–260.

Arculus, R.J., Pearce, J.A., Murton, B.J., Van der Laan, S.R., et al., 1992. Igneous stratigraphy and major element geochemistry of Holes 786A and 786B. In: Fryer, P., Pearce, J.A., Stokking, L.B. (Eds.), Proceedings of the Ocean Drilling Program, Scientific Results 125. Ocean Drilling Program, College Station, TX, pp. 143–169.

Asimow, P.D., Dixon, J.E., Langmuir, C.H., 2004. A hydrous melting and fractionation model for mid-ocean ridge basalts: applications to the Mid-Atlantic Ridge near the Azores. Geochemistry Geophysics Geosystems 5 (1), Q01E16. doi:10.1029/2003GC000568.

Bagci, U., Parlak, O., Höck, V., 2005. Whole-rock and mineral chemistry of cumulates from the Kizildag (Hatay) ophiolite (Turkey): clues for multiple magma generation during crustal accretion in the southern Neotethyan ocean. Mineralogical Magazine 69, 53–76.

Baragar, W.R.A., Lambert, M.B., Baglow, N., Gibson, I.L., 1989. Sheeted dykes of the Troodos ophiolite. In: Gibson, I.L., Malpas, J., Robinson, P.T., Xenophontos, C. (Eds.), Cyprus Crustal Study Project, Initial Reports Hole CY-4. Geological Survey of Canada, pp. 69–106. Paper 88-9.

Batanova, V.G., Sobolev, A.V., 2000. Compositional heterogeneity in subduction-related mantle peridotites, Troodos massif, Cyprus. Geology 28, 55–58. doi:10.1130/0091-7613(2000)28<55:CHISMP>2.0.CO;2.

Beccaluva, L., Coltorti, M., Premti, I., Saccani, E., Siena, F., Zeda, O., 1994. Mid-ocean ridge and supra-subduction affinities in the ophiolitic belts from Albania. Ofioliti 19, 77–96.

Beccaluva, L., Coltorti, M., Giunta, G., Siena, F., 2004. Tethyan vs. Cordilleran ophiolites: a reappraisal of distinctive tectono-magmatic features of supra-subduction complexes in relation to the subduction mode. Tectonophysics 393, 163–174. doi:10.1016/j.tecto.2004.07.034.

Bednarz, U., Schmincke, H.-U., 1994. Petrological and geochemical evolution of the northeastern Troodos extrusive series, Cyprus. Journal of Petrology 35, 489–523.

Bédard, J.H., Lauziere, K., Tremblay, A., Sangster, A., 1998. Evidence for forearc seafloor-spreading from the Betts Cove ophiolite, Newfoundland: oceanic crust of boninitic affinity. Tectonophysics 284, 233–245.

Blome, C.D., Irwin, W.P., 1985. Equivalent radiolarian ages from the ophiolite terrains of Cyprus and Oman. Geology 13, 401–404.

Bloomer, S.H., Taylor, B., MacLeod, C.J., Stern, R.J., Fryer, P., Hawkins, J.W., Johnson, L., 1995. Early arc volcanism and the ophiolite problem: a perspective from drilling in the Western Pacific. In: Taylor, B., Natland, J. (Eds.), Active Margins and Marginal Basins of the Western Pacific, 88. American Geophysical Union Geophysical Monograph, pp. 1–30.

Cameron, W.E., 1985. Petrology and origin of primitive lavas from the Troodos ophiolite, Cyprus. Contributions to Mineralogy and Petrology 89, 230–255.

Chan, G.H.-N., Malpas, J., Xenophontos, C., Lo, C.-H., 2007. Timing of subduction zone metamorphism during the formation and emplacement of Troodos and Baër-Bassit ophiolites: insights from ^{40}Ar–^{39}Ar geochronology. Geological Magazine 144, 797–810. doi:10.1017/S0016756807003792.

Çogulu, E., 1980. Roches filoniennes et les rodingites dans les serpentinites du massif du Kizildag (Hatay), Turquie. Arch. Sc. Genève 33, 269–279.

Çogulu, E., Delaloye, M., Vuagnat, M., Wagner, J.J., 1975. Some geochemical, geochronological and petrophysical data on the ophiolite massif from the Kizil Dagh, Hatay, Turkey. Comptes rendus des Séance de la Société de Physique et d'Histoire Naturelle de Genève 10, 141–150.

Cosca, M.A., Arculus, R.J., et al., 1998. $^{40}Ar/^{39}Ar$ and K–Ar geochronological age constraints for the inception and early evolution of the Izu–Bonin–Mariana arc system. The Island Arc 7, 579–595.

Cousens, B.L., Allan, J.F., Gorton, M.P., 1994. Subduction-modified pelagic sediment as the enriched component in back-arc basalts from the Japan Sea: Ocean Drilling Program Sites 797 and 794. Contributions to Mineralogy and Petrology 117, 421–434.

Crawford, A.J., Beccaluva, L., Serri, G., 1981. Tectono-magmatic evolution of the West Philippine–Mariana region and the origin of boninites. Earth and Planetary Science Letters 54, 346–356.

Crawford, A.J., Fallon, T.J., Green, D.H., 1989. Classification, petrogenesis and tectonic setting of boninites. In: Crawford, A.J. (Ed.), Boninites and Related Rocks. Unwin Hyman, London, pp. 1–49.

Crock, J.G., Lichte, F.E., 1982. Determination of rare earth elements in geologic materials by inductively couple argon plasma/atomic emission spectrometry. Analytical Chemistry 54, 1329–1332.

Delaloye, M., Wagner, J.J., 1984. Ophiolites and volcanic activity near the western edge of the Arabian plate. In: Dixon, J.E., Robertson, A.H.F. (Eds.), The Geological Evolution of the Eastern Mediterranean, 17. Geological Society, London, pp. 225–233. Special Publication.

Delaloye, M., Vuagnat, M., Wagner, J.J., 1977. K–Ar ages from the Kızıldag ophiolitic complex (Hatay, Turkey) and their interpretation. In: Biju-Duval, B., Montadert, L. (Eds.), International Symposium on the Structural History of the Mediterranean Basins, Split (Yugoslavia), pp. 73–78.

Delaloye, M., Piskin, O., Voldet, P., Vuagnat, M., Wagner, J.-J., 1979. Rare earth element concentrations in mafics from the Kizil Dag ophiolite (Hatay, Turkey). Schweizerische Mineralogische und Petrographische Mitteilungen 56, 67–73.

Dewey, J.F., Hempton, M.R., Kidd, W.S.F., Saroglu, F., Sengör, A.M.C., 1986. Shortening of continental lithosphere: the neotectonics of Eastern Anatolia—a young collision zone. In: Coward, M.P., Ries, A.C. (Eds.), Collision Zone Tectonics, vol. 19. Geological Society of London, pp. 3–36. Special Publication.

Dilek, Y., 2003. Ophiolite concept and its evolution. In: Dilek, Y., Newcomb, S. (Eds.), Ophiolite Concept and the Evolution of Geological Thought, vol. 373. Geological Society of America, pp. 1–16. Special Paper.

Dilek, Y., Delaloye, M., 1992. Structure of the Kizildag ophiolite, a slow-spread Cretaceous ridge segment north of the Arabian promontory. Geology 20, 19–22. doi:10.1130/0091-7613(1992)020.

Dilek, Y., Eddy, C.A., 1992. The Troodos (Cyprus) and Kizildag (S. Turkey) ophiolites as structural models for slow-spreading ridge segments. Journal of Geology 100, 305–322.

Dilek, Y., Flower, M.F.J., 2003. Arc-trench rollback and forearc accretion: 2. Model template for Albania, Cyprus, and Oman. In: Dilek, Y., Robinson, P.T. (Eds.), Ophiolites in Earth History, vol. 218. Geological Society of London, pp. 43–68. Special Publication.

Dilek, Y., Moores, E.M., 1990. Regional Tectonics of the Eastern Mediterranean ophiolites. In: Malpas, J., Moores, E.M., Panayiotou, A., Xenophontos, C. (Eds.), Ophiolites, Oceanic Crustal Analogues, Proceedings of the Symposium "Troodos 1987". The Geological Survey Department, Nicosia, Cyprus, pp. 295–309.

Dilek, Y., Thy, P., 1998. Structure, petrology and seafloor spreading tectonics of the Kizildag ophiolite, Turkey. In: Mills, R.A., Harrison, K. (Eds.), Modern Ocean Floor Processes and the Geological Record, 148. Geological Society, London, pp. 43–69. Special Publication.

Dilek, Y., Thy, P., 2006. Age and petrogenesis of plagiogranite intrusions in the Ankara Mélange, Central Turkey. Island Arc 15, 44–57. doi:10.1111/j.1440-1738.2006.00522.x.

Dilek, Y., Thy, P., Moores, E.M., Ramsden, T.W., 1990. Tectonic evolution of the Troodos ophiolite within the Tethyan framework. Tectonics 9, 811–823. doi:10.1029/TC009i004p00811.

Dilek, Y., Moores, E.M., Delaloye, M., Karson, J.A., 1991. Amagmatic extension and tectonic denudation in the Kizildag ophiolite, southern Turkey: implications for the evolution of Neotethyan oceanic crust. In: Peters, Tj. (Ed.), Ophiolite Genesis and Evolution of the Oceanic Lithosphere. In: Series in Petrology and Structural Geology, vol. 5. Kluwer Academic Publishers, The Netherlands, pp. 485–500.

Dilek, Y., Moores, E.M., Furnes, H., 1998. Structure of modern oceanic crust and ophiolites and implications for faulting and magmatism at oceanic spreading centers. In: Buck, R., Karson, J., Delaney, P., Lagabrielle, Y. (Eds.), Faulting and Magmatism at Mid-Ocean Ridges, vol. 106. Geophysical Monograph, American Geophysical Union, Washington, DC, 216–266.

Dilek, Y., Thy, P., Hacker, B., Grundvig, S., 1999. Structure and petrology of Tauride ophiolites and mafic dike intrusions (Turkey): Implications for the Neo-Tethyan ocean. Bulletin of the Geological Society of America 111, 1192–1216. doi:10.1130/0016-7606(1999)111<1192:SAPOTO>2.3.CO;2.

Dilek, Y., Shallo, M., Furnes, H., 2005. Rift–drift, seafloor spreading, and subduction tectonics of Albanian ophiolites. International Geology Review 47, 147–176. doi:10.2747/0020-6814.47.2.147.

Dilek, Y., Furnes, H., Shallo, M., 2007. Suprasubduction zone ophiolite formation along the periphery of Mesozoic Gondwana. Gondwana Research. doi:10.1016/j.gr.2007.01.005.

Dilek, Y., Furnes, H., Shallo, M., 2008. Geochemistry of the Jurassic Mirdita Ophiolite (Albania) and the MORB to SSZ evolution of a marginal basin oceanic crust. Lithos 100, 174–209. doi:10.1016/j.lithos.2007.06.026.

Dubertret, L., 1955. Géologie des roches vertes du nort-ouest de la Syrie et du Hatay (Turquie). Notes et Mèmoires. Moyen-Orient 6, 227 pp.

Duncan, R.A., Green, D.H., 1987. The genesis of refractory melts in the formation of oceanic crust. Contributions to Mineralogy and Petrology 96, 326–342.

Encarnacion, E., 2004. Multiple ophiolite generation preserved in the northern Philippines and the growth of an island arc complex. Tectonophysics 392, 103–130.

Erendil, M., 1984. Petrology and structure of the upper crustal units of the Kizildag ophiolite. In: Tekeli, O., Göncüoğlu, M.C. (Eds.), Geology of the Taurus Belt, Proceedings of the International Symposium on the Geology of the Taurus Belt 1983, Ankara, Turkey, pp. 269–284.

Flower, M.F.J., Levine, H.M., 1987. Petrogenesis of a tholeiite–boninite sequence from Ayios Mamas, Troodos ophiolite, evidence for splitting of a volcanic arc? Contributions to Mineralogy and Petrology 97, 509–524.

Gass, I.G., 1990. Ophiolites and oceanic lithosphere. In: Malpas, J., Moores, E.M., Panayiotou, A., Xenophontos, C. (Eds.), Ophiolites, Oceanic Crustal Analogues, Proceedings of the Symposium "Troodos 1987". The Geological Survey Department, Nicosia, Cyprus, pp. 1–10.

Godard, M., Dautria, J.-M., Perrin, M., 2003. Geochemical variability of the Oman ophiolite lavas: Relationship with spatial distribution and paleomagnetic directions. Geochemisty Geophysics Geosystems 4 (6). doi:10.1029/2002GC000452.

Gribble, R.F., Stern, R.J., Bloomer, S.H., Stüben, D., O, Hearn, T., Newman, S., 1996. MORB mantle and subduction components interact to generate basalts in the southern Mariana Trough back-arc basin. Geochimica et Cosmochimica Acta 60, 2153–2166.

Hacker, B.R., Mosenfelder, J.L., Gnos, E., 1996. Rapid emplacement of the Oman ophiolite, thermal and geochronologic constraints. Tectonics 15, 1230–1247.

Haraguchi, S., Ishii, T., 2007. Simultaneous boninitic and arc-tholeiitic volcanisms in the Izu forearc region during early arc volcanism, based on ODP Leg 125 Site 786. Contributions to Mineralogy and Petrology 153, 509–531. doi:10.1007/s00410-006-0164-6.

Hawkins, J.W., 2003. Geology of suprasubduction zones — implications for the origin of ophiolites. In: Dilek, Y., Newcomb, S. (Eds.), Ophiolite Concept and the Evolution of Geological Thought: Geological Society of America Special Paper, 373, pp. 227–268.

Hébert, R., Laurent, R., 1990. Mineral chemistry of the plutonic section of the Troodos ophiolite: new constraints for genesis of arc-related ophiolites. In: Malpas, J., Moores, E.M., Panayiotou, A., Xenophontos, C. (Eds.), Ophiolites, Oceanic Crustal Analogues, Proceedings of the Symposium "Troodos 1987". The Geological Survey Department, Nicosia, Cyprus, pp. 149–163.

Hickey, R., Frey, F.A., 1982. Geochemical characteristics of boninite series volcanics: implications for their source. Geochimica et Cosmochimica Acta 46, 2099–2115.

Hickey-Vargas, R., Reagan, M.K., 1987. Temporal variation of isotope and rare earth element abundance in volcanic rocks from Guam: implications for the evolution of the Mariana arc. Contributions to Mineralogy and Petrology 97, 497–508.
Hurst, S.D., Moores, E.M., Varga, R.J., 1994. Structural and geophysical expression of the Solea graben, Troodos ophiolite. Tectonics 13, 139–156.
Irvine, T.N., 1982. Terminology for layered intrusions. Journal of Petrology 23, 127–162.
Ishizuka, O., Uto, K., Yuasa, M., Hochstaedter, A.G., 2002. Volcanism in the earliest stage of back-arc rifting in the Izu–Bonin arc revealed by laser-heating $^{40}Ar/^{39}Ar$ dating. Journal of Volcanology and Geothermal Research 120, 71–85.
Ishizuka, O., Uto, K., Yuasa, M., 2003. Volcanic history of the back-arc region of the Izu–Bonin (Ogasawara) Arc. In: Larter, R.D., Leat, P.H. (Eds.), Intra-Oceanic Subduction Systems: Tectonic and Magmatic Processes, 219. Geological Society, London, pp. 187–205. Special Publication.
Johnson, D.M., Hooper, P.R., Conrey, R.M., 1999. XRF analysis of rocks and minerals for major and trace elements on a single low dilution Li-tetraborate fused bead. Advances in X-ray Analysis 41, 843–867.
Kamimura, A., Kasahara, J., Hino, R., Shinohara, M., Shiobara, H., 2002. Crustal structure study at the Izu–Bonin subduction zone around 31 degree N: Implication of serpentinized materials along the subduction plate boundary. Physics of the Earth and Planetary Interiors 131, 289–313.
Karson, J.A., 1998. Internal structure of oceanic lithosphere: a perspective from tectonic windows. In: Mills, R.A., Harrison, K. (Eds.), Modern Ocean Floor Processes and the Geological Record, 148. Geological Society, London, pp. 177–218. Special Publication.
Kilinç, A., Carmichael, I.S.E., Rivers, M.L., Sack, R.O., 1983. The ferric–ferrous ratio of natural silicate liquids equilibrated in air. Contributions to Mineralogy and Petrology 83, 136–140.
Klaus, A., Taylor, B., Moore, G.F., Murakami, F., Okamura, Y., 1992. Back-arc rifting in the Izu–Bonin island arc: structural evolution of Hachijo and Aogo Shima rifts. The Island Arc 1, 16–31.
Krogh, T.E., 1973. A low contamination method for hydrothermal decomposition of zircon and extraction of U and Pb for isotopic age determinations. Geochimica et Cosmochimica Acta 37, 485–494.
Langmuir, C.H., Klein, E.M., Plank, T., 1992. Petrological systematics of mid-ocean ridge basalt: constraints on melt generation beneath ocean ridges. In: Morgan, J.P., Blackman, D.K., Sinton, J.M. (Eds.), Mantle Flow and Melt Generation at Mid-Ocean Ridges: American Geophysical Union Geophysical Monograph, vol. 71, pp. 183–280.
Laurent, R., Delaloye, M., Vuagnat, M., Wager, J.J., 1980. Composition of parental basaltic magma in ophiolites. In: Panayiotou (Ed.), Ophiolites, Proceedings International Ophiolite Symposium. Geological Survey Department, Nicosia, Cyprus, pp. 172–181.
Ludwig, K.R., 1990. PBDAT for MS-DOS: a computer program for IBM-PC compatibles for processing Pb–U–Th isotope data version 1.07. United States Geological Survey Open-File Report 88-542.
Ludwig, K.R., 2003. Mathematical–statistical treatment of data and errors for Th-230/U geochronology. Uranium-Series Geochemistry. Reviews in Minerology and Geochemistry 52, 631–656.
Lytwyn, J.N., Casey, J.F., 1993. The geochemistry and petrogenesis of volcanic and sheeted dikes from Hatay (Kizildag) ophiolite, southern Turkey: possible formation with the Troodos ophiolite, Cyprus, along fore-arc spreading centers. Tectonophysics 223, 237–272.
Malpas, J., Langdon, G., 1984. Petrology of upper pillow lava suite, Troodos ophiolite, Cyprus. In: G ass, I.G., L ippard, S.J., Shelton, A.W. (Eds.), Special Publication, vol. 13. Geological Society, London, pp. 155–167.
Malpas, J., Brace, T., Dunsworth, S.M., 1989. Structural and petrological relationships of the CY-4 drill hole of the Cyprus Crustal Study Project. In: Gibson, I.L., Malpas, J., Robinson, P.T., Xenophontos, C. (Eds.), Initial Report, Hole CY-4. Geological Survey of Canada, pp. 39–67. Papers 88-9.
McCulloch, M.T., Cameron, W.E., 1983. Nd–Sr isotopic study of primitive lavas from the Troodos ophiolite, Cyprus: evidence for a subduction-related setting. Geology 11, 727–731.
Morris, A., Anderson, M.W., Robertson, A.H.F., Al-Riyami, K., 2002. Extreme tectonic rotations within an eastern Mediterranean ophiolite (Baër-Bassit, Syria). Earth and Planetary Science Letters 202, 247–261.
Mukasa, S.B., Ludden, J.N., 1987. Uranium–lead ages of plagiogranites from the Troodos ophiolite, Cyprus, and their tectonic significance. Geology 15, 825–828.
Nishizawa, A., Kaneda, K., Nakanishi, A., Takahashi, N., Kodaira, S., 2006. Crustal structure of the ocean–island arc transition at the mid Izu–Ogasawara (Bonin) arc margin. Earth Planets Space 58, e33–e36.
Niu, Y., Batiza, R., 1991. An empirical method for calculating melt compositions produced beneath mid-ocean ridges: application for axis and off-axis (Seamounts) melting. Journal of Geophysical Research 96, 21753–21777.
Panjasawatwong, Y., Danyushevsky, L.V., Crawford, A.J., Harris, K.L., 1995. An experimental study of the effects of melt composition on plagioclase–melt equilibria at 5 and 10 kbar: implications for the origin of magmatic high-An plagioclase. Contributions to Mineralogy and Petrology 118, 420–432.
Parrot, J.F., 1980. The Baër-Bassit (Northwestern Syria) ophiolitic area. Ofioliti 2, 279–295.
Pearce, J.A., Parkinson, I.J., 1993. Trace element models for mantle melting: application to volcanic arc petrogenesis. In: Prichard, H.M., Alabaster, T., Harris, N.B.W., Neary, C.R. (Eds.), Magmatic Processes and Plate Tectonics, 76. Geological Society, London, pp. 373–403. Special Publication.
Pearce, J.A., Van der Laan, S.R., Arculus, R.J., Murton, B.J., Ishii, T., Peate, D.W., Parkinson, I.J., 1992. Boninite and harzburgite from Leg 125 (Bonin–Mariana forearc): a case study of magma genesis during the initial stages of subduction. In: Fryer, P., Pearce, J.A., Stokking, L.B. (Eds.), Proceedings of the Ocean Drilling Program, Scientific Results. Ocean Drilling Program, College Station, Texas, pp. 623–659.
Piskin, O., Delaloye, M., Moritz, R., Wagner, J.J., 1990. Geochemistry and geothermometry of the Hatay Complex, Turkey: implications for the genesis of the ophiolite sequence. In: Malpas, J., Moores, E.M., Panayiotou, A., Xenophontons, C. (Eds.), Ophiolites, Oceanic Crustal Analogues. Geological Survey Department, Nicosia, Cyprus, pp. 329–338.
Polat, A., Casey, J.F., Kerrich, R., 1996. Geochemical characteristics of accreted material beneath the Pozanti–Karsanti ophiolite, Turkey: intra-oceanic detachment, assembly and obduction. Tectonophysics 263, 249–276. doi:10.1016/S0040-1951(96)00026-1.
Portnyagin, M.V., Danyushevsky, L.V., Kamenetsky, V.S., 1997. Coexistence of two distinct mantle sources during formation of ophiolites: a case study of primitive pillow-lavas from the lowest part of the volcanic section of the Troodos ophiolite, Cyprus. Contributions to Mineralogy and Petrology 128, 287–301.
Rautenschlein, M., Jenner, G.A., Hertogen, J., Hofmann, A.W., Kerrich, R., Schmincke, H.-U., White, W.M., 1985. Isotopic and trace element composition of volcanic glasses from Akaki canyon, Cyprus: implications for the origin of Troodos ophiolite. Earth and Planetary Science Letters 75, 369–383.
Ricou, L.E., 1971. Le croissant ophiolitique péri-arabe. Une ceinture de nappes mises en place au Crétacé supérieur. Revue de Géographie Physique et de Physique Geologie et Dynamique 13/4, 327–350.
Robertson, A.H.F., 1986. Geochemistry and tectonic implications of metalliferous and volcanoclastic sedimentary rocks associated with late cretaceous ophiolitic extrusives in the Hatay area, southern Turkey. Ofioliti 11, 121–140.
Robertson, A.H.F., 1998. Mesozoic–Tertiary tectonic evolution of the easternmost Mediterranean area: integration of marine and land evidence. In: Robertson, A.H.F., Emeis, K.C., Richetr, C., Camerlenghi, A. (Eds.), Proceedings of the Ocean Drilling Program, Scientific Results, vo. 160, pp. 723–782.
Robertson, A.H.F., 2002. Overview of the genesis and emplacement of Mesozoic ophiolites in the Eastern Mediterranean Tethyan region. Lithos 65, 1–67.
Robinson, P.T., Malpas, J., 1990. The Troodos ophiolite of Cyprus: new perspectives on its origin and emplacement. In: Malpas, J., Moores, E.M., Panayiotou, A., Xenophontos, C. (Eds.), Ophiolites, Oceanic Crustal Analogues, Proceedings of the Symposium "Troodos 1987". The Geological Survey Department, Nicosia, Cyprus, pp. 13–26.
Robinson, P.T., Melson, W.G., O, Hearn, T., Schmincke, H.-U., 1983. Volcanic glass compositions of the Troodos ophiolite, Cyprus. Geology 11, 400–404.
Selçuk, H. 1981. Étude géologique de la partie méridionale du Hatay (Turquie). Thèse de Doctorat, Université de Genève, Suisse (unpublished).
Shervais, J.W., 2001. Birth, death, and resurrection: the life cycle of suprasubduction zone ophiolites. Geochemistry Geophysics Geosystems 2, Paper Number 2000GC000080.
Sobolev, A.V., Portnyagin, M.V., Dimitriev, L.V., Tsameryan, O.P., Danyushevsky, L.V., Kononkova, N.N., Shimizu, N., Robinson, P.T., 1993. Petrology of ultramafic lavas and associated rocks of the Troodos massif, Cyprus. Petrology 1, 379–412.
Stacy, J.S., Kramers, J.D., 1975. Approximation of terrestrial lead isotope evolution by a two stage model. Earth and Planetary Science Letters 26, 207–221.
Staudigel, H., Tauxe, L., Gee, J.S., Bogaard, P., Haspels, J., Kale, G., Leenders, A., Meijer, P., Swaak, B., Tuin, M., Van Soest, M.C., Verdurmen, E.A.Th., Zevenhuizen, A., 1999. Geochemistry and intrusive directions in sheeted dikes in the Troodos ophiolite: implications for mid-ocean ridge spreading centers. Geochemistry Geophysics Geosystems 1 (1).
Steiger, R.H., Jaeger, E., 1977. Subcommission on geochronology: convention on the use of decay constants in geo- and cosmochronology. Earth and Planetary Science Letters 36 , 359–362.
Stern, R.J., 2004. Subduction initiation: spontaneous and induced. Earth and Planetary Science Letters 226, 275–292.
Stern, R.J., Bloomer, S.H., 1992. Subduction zone infancy: examples from the Eocene Izu–Bonin–Mariana and Jurassic California arcs. Bulletin of the Geological Society of America 104, 1621–1636.
Stern, R.J., Bloomer, S.H., Lin, P.-N., Smoot, N.C., 1989. Submarine arc volcanism in the southern Mariana Arc as an ophiolite analogue. Tectonophysics 168, 151–170.
Stern, R.J., Fouch, M.J., Klemperer, S., 2003. An overview of the Izu–Bonin–Mariana subduction factory. In: Eiler, J.M. (Ed.), Inside the Subduction Factory. In: Geophysical Monograph, vol. 138. American Geophysical Union, Washington DC, pp. 175–222.
Stolper, E., Newman, S., 1994. The role of water in the petrogenesis of Mariana Trough magmas. Earth and Planetary Science Letters 121, 293–325.
Straub, S.M., 2003. The evolution of the Izu–Bonin–Mariana volcanic arcs (NW Pacific) in terms of major elements. Geochemistry Geophysics Geosystems 4 (2), 1018. doi:10.1029/2002GC000357.
Sun, S.-S., McDonough, W.F., 1989. Chemical and isotopic systematics of oceanic basalts: implications for mantle composition and processes. In: Saunders, A., Norry, M.J. (Eds.), Magmatism in the Ocean Basins, 42. Geological Society, London, pp. 313–345. Special Publication.
Takahashi, E., Shimazaki, T., Tsuzaki, Y., Yoshida, H., 1993. Melting study of a peridotite KLB-1 to 6.5 GPA, and the origin of basaltic magmas. Philosophical Transactions of the Royal Society of London A 342, 105–120.
Takahashi, N., Kodaira, S., Klemperer, S.L., Tatsumi, Y., Kaneda, Y., Suyehiro, K., 2007. Crustal structure and evolution of the Mariana intra-oceanic island arc. Geology 35, 203–206.
Tatsumi, Y., Hamilton, D.L., Nesbitt, R.W., 1986. Chemical characteristics of fluid released from a subducted lithosphere and origin of arc magmas: evidence from high-pressure experiments and natural rocks. Journal of Volcanology and Geothermal Research 29, 293–309.
Taylor, B., 1992. Rifting and the volcanic–tectonic evolution of the Izu–Bonin–Mariana Arc. In: Taylor, B., Fujioka, K., et al. (Eds.), Proceedings of the Ocean Drilling Program, Scientific Results, 126, pp. 627–651.
Taylor, R.N., Nesbitt, R.W., 1988. Light rare-earth enrichment of supra subduction-zone mantle: evidence from the Troodos ophiolite, Cyprus. Geology 16, 448–451.
Taylor, B., Klaus, A., Brown, G.R., Moore, G.F., 1991. Structural development of Sumisu Rift, Izu–Bonin Arc. Journal of Geophysical Research 96, 16113–16129.

Tekeli, O., Erendil, M., 1986. Geology and petrology of the Kizildag ophiolite (Hatay). Bulletin of the Mineral Research and Exploration Institute, Turkey (MTA) 21, 21–37.
Thuziat, R., Whitechurch, H., Montigny, R., Juteau, T., 1981. K–Ar dating of some infra-ophiolitic metamorphic soles from the Eastern Mediterranean: new evidence for oceanic thrusting before obduction. Earth and Planetary Science Letters 52, 301–310.
Thy, P., 1987. Petrogenetic implications of mineral crystallization trends of Troodos cumulates, Cyprus. Geological Magazine 124, 415–430.
Thy, P., Esbensen, K.H., 1993. Seafloor spreading and the ophiolitic sequences of the Troodos Complex: A principal component analysis of lava and dike compositions. Journal of Geophysical Research 98, 11799–11805.
Thy, P., Xenophontos, C., 1991. Crystallization orders and phase chemistry of glassy lavas from the pillow sequences, Troodos ophiolite, Cyprus. Journal of Petrology 32, 403–428.
Thy, P., Schiffman, P., Moores, E.M., 1989. Igneous mineral stratigraphy and chemistry of the Cyprus Crustal Study Project drill core in the plutonic sequences of the Troodos ophiolite. In: Gibson, I.L., Malpas, J., Robinson, P.T., Xenophontos, C. (Eds.), Cyprus Crustal Study Project, Hole CY-4: Geological Survey of Canada, Paper 88-9, pp. 147–185.
Tinkler, C., Wagner, J.J., Delaloye, M., Selçuk, H., 1981. Tectonic history of the Hatay ophiolites (South Turkey) and their relations with the Dead Sea Rift. Tectonophysics 72, 23–41.
Van der Lann, S.R., Arculus, R.L., Pearce, J.A., Murton, B.J., 1992. Petrography, mineral chemistry and phase relations of the basement boninite series of Site 786, Izu–Bonin forearc. Proceedings of the Ocean Drilling Program Scientific Results 125, 171–201.
Vuagnat, M., Çogulu, E., 1967. Quelques reflextions sur le massif basique–ultrabasique du Kizildag, Hatay, Turquie. Comptes rendus de la Société de Physique et d'Histoire Naturelle de Genève 2/3, 210–216.
Wager, L.R., Brown, G.M., Wadsworth, W.J., 1960. Types of igneous cumulates. Journal of Petrology 1, 73–85.
Wakabayashi, J., Dilek, Y., 2003. What constitutes 'emplacement' of an ophiolite?: Mechanisms and relationship to subduction initiation and formation of metamorphic soles. In: Dilek, Y., Robinson, P.T. (Eds.), Ophiolites in Earth History, 218. Geological Society, London, pp. 427–448. Special Publication.